NAVAL POSTGRADUATE SCHOOL
Monterey, California

THESIS

A FRAMEWORK FOR DESIGNING OPTIMAL SPACECRAFT FORMATIONS

by

Jeffery T. King

September 2002

Thesis Advisor:	I. Michael. Ross
Second Reader:	Fariba Fahroo

Approved for public release; distribution is unlimited

THIS PAGE INTENTIONALLY LEFT BLANK

REPORT DOCUMENTATION PAGE			Form Approved OMB No. 0704-0188

Public reporting burden for this collection of information is estimated to average 1 hour per response, including the time for reviewing instruction, searching existing data sources, gathering and maintaining the data needed, and completing and reviewing the collection of information. Send comments regarding this burden estimate or any other aspect of this collection of information, including suggestions for reducing this burden, to Washington headquarters Services, Directorate for Information Operations and Reports, 1215 Jefferson Davis Highway, Suite 1204, Arlington, VA 22202-4302, and to the Office of Management and Budget, Paperwork Reduction Project (0704-0188) Washington DC 20503.

1. AGENCY USE ONLY *(Leave blank)*	2. REPORT DATE September 2002	3. REPORT TYPE AND DATES COVERED Master's Thesis

4. TITLE AND SUBTITLE. A Framework For Designing Optimal Spacecraft Formations	5. FUNDING NUMBERS
6. AUTHOR(S)	
7. PERFORMING ORGANIZATION NAME(S) AND ADDRESS(ES) Naval Postgraduate School Monterey, CA 93943-5000	8. PERFORMING ORGANIZATION REPORT NUMBER
9. SPONSORING /MONITORING AGENCY NAME(S) AND ADDRESS(ES) N/A	10. SPONSORING/MONITORING AGENCY REPORT NUMBER

11. SUPPLEMENTARY NOTES The views expressed in this thesis are those of the author and do not reflect the official policy or position of the Department of Defense or the U.S. Government.

12a. DISTRIBUTION / AVAILABILITY STATEMENT Approved for public release; distribution is unlimited	12b. DISTRIBUTION CODE

13. ABSTRACT *(maximum 200 words)*

This thesis presents a new approach to solving a class of problems arising in the design of satellite swarms. Using the fundamentals of optimal control theory, a framework is developed that captures the essence of "concurrent" design and control of spacecraft formations. This framework is used to articulate a variety of formations including the notion of an aperiodic formation. Additionally, formations that require active control are presented along with their corresponding thrust profile. Based on a deliberate problem formulation, which includes mass as a state variable, it is shown that the numerical approach easily handles nonlinearities. Using the general-purpose dynamic optimization software, DIDO, this thesis demonstrates how a minimum-propellant formation configuration can be easily designed for satellite swarms *without the use of any analytical results*. If a zero-propellant configuration does not exist, then this method automatically determines the minimum fuel and the associated controls required to maintain the configuration. This thesis lends credence to the notion of numerically searching for minimum-fuel formation configurations for spacecraft swarms subject to *arbitrary* nonlinear dynamics. Thus, practical formations may be designed and controlled using this method.

14. SUBJECT TERMS Satellite Formation, Formation Design, Optimal Design, DIDO, Swarm	15. NUMBER OF PAGES 97
	16. PRICE CODE

17. SECURITY CLASSIFICATION OF REPORT	18. SECURITY CLASSIFICATION OF THIS PAGE	19. SECURITY CLASSIFICATION OF ABSTRACT	20. LIMITATION OF ABSTRACT
Unclassified	Unclassified	Unclassified	UL

NSN 7540-01-280-5500 Standard Form 298 (Rev. 2-89)
Prescribed by ANSI Std. 239-18

THIS PAGE INTENTIONALLY LEFT BLANK

Approved for public release; distribution is unlimited

FRAMEWORK FOR DESIGNING OPTIMAL SPACECRAFT FORMATIONS

Jeffery T. King
Lieutenant, United States Navy
B.S., United States Naval Academy, 1993

Submitted in partial fulfillment of the
requirements for the degree of

**MASTER OF SCIENCE IN
ASTRONAUTICAL ENGINEERING**

from the

**NAVAL POSTGRADUATE SCHOOL
September 2002**

Author: Jeffery T. King

Approved by: I. Michael Ross
Thesis Advisor

Fariba Fahroo
Second Reader

Max F. Platzer
Chairman, Department of Aeronautics and Astronautics

THIS PAGE INTENTIONALLY LEFT BLANK

ABSTRACT

This thesis presents a new approach to solving a class of problems arising in the design of satellite swarms. Using the fundamentals of optimal control theory, a framework is developed that captures the essence of "concurrent" design and control of spacecraft formations. This framework is used to articulate a variety of formations including the notion of an aperiodic formation. Additionally, formations that require active control are presented along with their corresponding thrust profile. Based on a deliberate problem formulation, which includes mass as a state variable, it is shown that the numerical approach easily handles nonlinearities. Using the general-purpose dynamic optimization software, DIDO, this thesis demonstrates how a minimum-propellant formation configuration can be easily designed for satellite swarms *without the use of any analytical results*. If a zero-propellant configuration does not exist, then this method automatically determines the minimum fuel and the associated controls required to maintain the configuration. This thesis lends credence to the notion of numerically searching for minimum-fuel formation configurations for spacecraft swarms subject to *arbitrary* nonlinear dynamics. Thus, practical formations may be designed and controlled using this method.

THIS PAGE INTENTIONALLY LEFT BLANK

TABLE OF CONTENTS

I. INTRODUCTION 1

II. GENERAL FRAMEWORK 3
- A. PROBLEM DEFINITION[19] 3
  - 1. Reference Frame 6
- B. SOLVING OPTIMAL CONTROL PROBLEMS 7
  - 1. Necessary Conditions for Optimality 8
  - 2. Scaling 10
  - 3. Unique Issues for Periodic Problems 11
- C. VALIDATING SOLUTIONS 12
  - 1. Numeric Propagators 12
  - 2. Commercial Software 13
  - 3. Previously Discovered Solutions 14

III. CIRCULAR REFERENCE ORBIT 15
- A. PROBLEM DEFINITION 15
- B. EQUATIONS OF MOTION 17
- C. C-W SOLUTIONS 17
  - 1. C-W Circular Solution 18
  - 2. C-W Projected Circular Solution 18
- D. NON-LINEAR TWIST 18
  - 1. New Equations of Motion 20
  - 2. Circular Formation Solution with New EOM 20
  - 3. Projected Circular Formation Solution with New EOM 24
- E. VALIDATION OF SOLUTIONS 27

IV. ELLIPTIC REFERENCE ORBIT 31
- A. PROBLEM DEFINITION 31
- B. EQUATIONS OF MOTION 32
- C. NATURAL SOLUTIONS 35
  - 1. Natural Formation for $e = 0.5$ 35
  - 2. Natural Formation for $e = 0.3$ 39
  - 3. Natural Formation for $e = 0.7$ 44
- D. FORCED SOLUTIONS 46
  - 1. Forced Circular Formation 46
  - 2. Forced Projected Circular Formation 51
- E. VALIDATION OF SOLUTIONS 55
  - 1. Natural Formation for $e = 0.5$ 57
  - 2. Natural Formation for $e = 0.3$ 58
  - 3. Natural Formation for $e = 0.7$ 59
  - 4. Forced Circular Formation 59
  - 5. Forced Projected Circular Formation 60

V. UNRESOLVED ISSUES 63
A. OPTIMAL PERIOD VS. ORBITAL PERIOD 63
B. SWITCHING FUNCTION : DERIVED VS. DIDO SOLUTION 64
C. J2 PERTURBATIONS 65
1. Linear J_2 terms. 65
2. Non-linear J_2 terms. 65
3. Comparison Between Sets of Equations. 66
VI. CONCLUSIONS AND FUTURE WORK 71
A. CONCLUSIONS 71
B. OPPORTUNITIES FOR FUTURE WORK 71
LIST OF REFERENCES 73
INITIAL DISTRIBUTION LIST 77

LIST OF FIGURES

Figure II-1 Formation Reference Frame 6
Figure III-1 Circular Formation Using New Equations of Motion.....21
Figure III-2 Radial vs. Along-Track Motion for a Circular Formation.....22
Figure III-3 Cross-Track vs. Radial Motion for a Circular Formation.....22
Figure III-4 Cross-Track vs. Along-Track Motion for a Circular Formation.....23
Figure III-5 Thrust Profile for Circular Formation with New EOM 23
Figure III-6 Projected Circular Formation Using New Equations of Motion 25
Figure III-7 Radial vs. Along-Track Motion for a Projected Circular Formation.....25
Figure III-8 Cross-Track vs. Radial Motion for a Projected Circular Formation.....26
Figure III-9 Cross-Track vs. Along-Track Motion for a Projected Circular Formation 26
Figure III-10 Thrust Profile for Projected Circular Formation with New EOM 27
Figure III-11 Circular Solution Over 50 Orbits.....28
Figure III-12 Projected Circular Solution Over 50 Orbits.....29
Figure IV-1 3-Dimensional Formation Trajectory for $e = 0.5$ Natural Formation 37
Figure IV-2 Radial vs. Along-Track Motion for $e = 0.5$ Natural Formation.....37
Figure IV-3 Cross-Track vs. Radial Motion for $e = 0.5$ Natural Formation.....38
Figure IV-4 Cross-Track vs. Along-Track Motion for $e = 0.5$ Natural Formation 38
Figure IV-5 Thrust Profile for $e = 0.5$ Natural Formation.....39
Figure IV-6 3-Dimensional Formation Trajectory for $e = 0.3$ Natural Formation 41
Figure IV-7 Radial vs. Along-Track Motion for $e = 0.3$ Natural Formation 42
Figure IV-8 Cross-Track vs. Radial Motion for $e = 0.3$ Natural Formation 42
Figure IV-9 Cross-Track vs. Along-Track Motion for $e = 0.3$ Natural Formation.....43
Figure IV-10 Thrust Profile for $e = 0.3$ Natural Formation 43
Figure IV-11 Radial vs. Along-Track Motion for $e = 0.7$ Natural Formation.....45
Figure IV-12 Cross-Track vs. Along-Track Motion for $e = 0.7$ Natural Formation 45
Figure IV-13 Forced Circular Formation for $e = 0.3$ 47
Figure IV-14 Forced Circular Formation Radial vs. Along Track Motion.....48
Figure IV-15 Forced Circular Formation Cross-Track vs. Radial Motion 48

Figure IV-16 Forced Circular Formation Cross-Track vs. Along-Track Motion 49
Figure IV-17 Forced Circular Formation Control Thrust Profile 49
Figure IV-18 Relative Angular Momentum Vector for the C-W Circular Formation 50
Figure IV-19 Relative Angular Momentum Vector for the Forced Circular Formation 51
Figure IV-20 Forced Projected Circular Formation for $e = 0.3$ 52
Figure IV-21 Forced Projected Circular Formation Radial vs. Along Track Motion 53
Figure IV-22 Forced Projected Circular Formation Cross-Track vs. Radial Motion 53
Figure IV-23 Forced Projected Circular Formation Cross-Track vs. Along-Track Motion..54
Figure IV-24 Forced Projected Circular Formation Control Thrust Profile 54
Figure IV-25 Switching Functions for Control Thrust 56
Figure IV-26 Natural Formation with $e = 0.5$ Over 50 Orbits.....57
Figure IV-27 Natural Formation with $e = 0.3$ Over 50 Orbits 58
Figure IV-28 Forced Circular Formation over 50 Orbits.....59
Figure IV-29 Forced Projected Circular Formation over 50 orbits 61
Figure V-1 Relative Accelerations Due to J2 at 28.5º Inclination 67
Figure V-2 Relative Accelerations Due to J2 at 45º Inclination 68
Figure V-3 Relative Accelerations Due to J2 at 63.4º Inclination 68
Figure V-4 Error in Linear Equations at 28.5º Inclination 69
Figure V-5 Error in Linear Equations at 45º Inclination 69
Figure V-6 Error in Linear Equations at 63.4º Inclination 70

LIST OF TABLES

Table III-1 Constraints for Circular Formation 21
Table III-2 Constraints for Projected Circular Formation 24
Table III-3 Propagation Results for Analytical C-W Circular Solution 29
Table III-4 Propagation Results for Circular Formation 30
Table III-5 Propagation Results for Projected Circular Formation 30
Table IV-1 Constraints for Natural Formation with $e = 0.5$ 36
Table IV-2 Constraints for Natural Formation with $e = 0.3$ 41
Table IV-3 Constraints for Natural Formation with $e = 0.7$ 44
Table IV-4 Constraints for Forced Circular Formation 47
Table IV-5 Constraints for Forced Projected Circular Formation 52
Table IV-6 Propagation Results for Natural Formation with $e = 0.5$ 57
Table IV-7 Propagation Results for Natural Formation with $e = 0.3$ 58
Table IV-8 Propagation Results for Forced Circular Formation 60
Table IV-9 Propagation Results for Forced Projected Circular Formation 61
Table V-1 Differing Costs for Forced Circular Solutions 63
Table V-2 Differing Costs for Forced Projected Circular Solutions 64

THIS PAGE INTENTIONALLY LEFT BLANK

LIST OF SYMBOLS

Subscripts:

$f, 0$ - Final or Initial conditions, respectively

u, l - Upper or Lower bounds, respectively

Superscripts:

N - Inertial Reference Frame

B - Formation Reference Frame

Variables:

Dots denote the time derivative of a given variable.

^ denotes a unit vector direction.

a - Semi-major axis of reference orbit

$\mathbf{a}_{J_2}$ - Accelerations due to J_2 effects

$\mathbf{a}_p$ - Accelerations of swarm satellite due to perturbations

$\mathbf{a}_T$ - Accelerations due to thrusting or control

$\mathbf{c}$ - User-defined configuration metric

$\mathbf{d}$ - Distance

e - Eccentricity of reference orbit

$\mathbf{e}$ - Events function

F - Lagrange Cost Functional

$\mathbf{g}$ - Path function

$\mathbf{f}$ - Right-hand side of Dynamic equations

H - Hamiltonian

$\mathbf{h}$ - Orbital Angular Momentum vector

h - Magnitude of $\mathbf{h}$

J - Scalar performance measure

k - See Equation (4.23)

L - Lagrangian or augmented function

m - Mass of spacecraft

n - Mean motion of reference orbit

N_c - Number of configuration metrics utilized

N_s - Number of spacecraft in formation

$\mathbf{p}$ - Generic vector of constant design parameters

$\mathbf{r}$ - Relative radius vector

r - Magnitude of $\mathbf{r}$

$\mathbf{R}$ - Inertial radius vector

R - Magnitude $\mathbf{R}$

$\mathbf{T}$ - Thrust vector (subscripts denote axis)

T - Magnitude $\mathbf{T}$

$\mathbf{u}$ - Control vector

v_e - Characteristic velocity

$\mathbf{x}$ - State vector for a given spacecraft

$\mathbf{y}$ - State vector of reference satellite or point

ε - Arbitrary tolerance value

λ - Lagrange multipliers for dynamic constraints

φ - Lagrange multipliers for static constraints

μ - Gravitational parameter of Earth

ν - True anomaly

$\boldsymbol{\omega}$ - Angular velocity vector

ω - Argument of Perigee

τ - Time

Ω - Right Ascension of the Ascending Node

$\mathbb{R}^N$ - N-dimensional real space

THIS PAGE INTENTIONALLY LEFT BLANK

ACKNOWLEDGMENTS

First and foremost, to my Lord, Jesus Christ for giving me the ability and opportunity.

To my Thesis Advisor for seeing the potential and igniting the spark.

To Scott Josselyn, Jim Ross, Rob Stevens, and Jon Strizzi for sharing the lab and for the invaluable advice and friendship.

To my children, Megan and Joshua, for enduring the many hours of "Papa is still at work."

Finally, to my wife, Sandra, for being the most wonderful gift ever given to a man. Thank you for your unending support and encouragement.

THIS PAGE INTENTIONALLY LEFT BLANK

I. INTRODUCTION

The concept of distributing the functionality of larger satellites among smaller, cooperative satellites has been seriously considered for assorted space missions to accomplish goals that are not possible or very difficult to do with a single satellite.[1,2,3] The current trend in satellite design is toward using smaller, more capable satellites in cooperative formations or distributed arrays.[4,5]

An extremely critical issue in architecting satellite swarms is the formation configuration. Arguably, the main feasibility criterion in the architecture of satellite swarms is the design of globally-minimum-fuel configurations. This simply follows from the fact that fuel for orbiting spacecraft comes at a very high premium and could significantly offset any other advantage held by a swarm configuration. Thus, there is a need to determine zero-propellant formation configurations (if they exist) and methods for controlling the formation with little or no propellant. It is well known that a family of zero-propellant circular and elliptic formations exists when the spacecraft are subject only to an inverse-square gravity field.[6,7] However, these formations tear apart in the presence of "disturbing" effects such as J_2. Thus, a search for invariant relative orbits or formations (if they exist) goes on.[8] Another effect that must be accounted for is a non-zero eccentricity of the reference orbit.[9] Unlike the J_2 disturbance, an error in eccentricity can be controlled by a one-time expenditure of propellant. This is based on the observation that the J_2 disturbance is an error in the dynamical model whereas the error in eccentricity is one of initial conditions. The error in eccentricity does not fully address the problem since in many applications it is desirable to have formations for every eccentricity (and not just small eccentricities). Hence, the "real" problem is to find formations in the presence of the totality of (modelable) deterministic forces. If such formations do not exist naturally, then it is imperative that the minimum-fuel formation configuration be determined. The total fuel consumption of a formation over its lifetime then establishes the practical feasibility of a swarm architecture. There are some opinions[10] suggesting that minimum-fuel configurations exist and that they do not offset the advantages offered by other performance metrics. However, there appears to be no

general-purpose method published in the open literature on how to find these minimum-fuel configurations subject to arbitrary forces.

This thesis presents a general problem algorithm for finding optimal formations and shows that a very natural setting for solving this problem is (nonlinear) optimal control theory. In particular, these ideas are formulated by using elements from *optimal periodic control* theory with *partially periodic states*.[11] The Legendre pseudospectral technique is applied to numerically solve this problem (see Reference 12 and the references contained therein). Because of the Covector Mapping Theorem,[13] this technique is neither a direct nor an indirect method. Rather, it provides all the ease of a direct method while providing the accuracy of an indirect method. This method is implemented using the general-purpose software package, DIDO,[14] which has been used extensively over the past few years to solve a myriad of complex optimal control problems.

The applicability of optimal control theory to satellite formation was not known at the outset of the thesis work presented here. For this reason, the research style chosen was a building-block approach. First, optimal control theory had to be demonstrated as an appropriate framework for a simplified model and then complexity would be added incrementally.

A model simply captures the essential aspects from a certain point of view and simplifies or ignores the rest. The so-called Hill-Clohessy-Wiltshire[15] (C-W) equations were chosen as the first model specifically because the solutions were known. This allowed a validation of the method before embarking upon more complicated models. The second model was chosen to address the eccentric reference orbit. To do this, a *nonlinear version* of the linearized equations[16,17,18] was used for the dynamical model *without the presumption of a solution*.

II. GENERAL FRAMEWORK

A. PROBLEM DEFINITION[19]

The notion of a swarm can be defined by stating that a group of satellites are said to be in *formation* if a given configuration metric $\mathbf{c}\left(\left\{\mathbf{x}^i\right\}\right)$ is bounded,

$$\mathbf{c}_l \le \mathbf{c}(\{\mathbf{x}^i\}) \le \mathbf{c}_u \qquad \mathbf{c} \in \mathbb{R}^{N_c} \tag{2.1}$$

where $\mathbf{x}^i$ denotes the state of the ith spacecraft at time τ. This state can be the usual position-velocity state or any other set (e.g. orbital elements).

The dynamics of a swarm of N_s spacecraft are given in some coordinate system by,

$$\dot{\mathbf{x}}^i = \mathbf{f}(\mathbf{x}^i, \mathbf{u}^i, \tau; \mathbf{p}) \qquad i = 1 \ldots N_s \tag{2.2}$$

If the distance between any two satellites, $d(\mathbf{x}^i, \mathbf{x}^j)$, is chosen as the metric, then the swarm is said to be in formation if

$$d_l^{i,j} \le d(\mathbf{x}^i, \mathbf{x}^j) \le d_u^{i,j} \qquad \forall \tau \tag{2.3}$$

where d_l and d_u define the smallest and largest allowable separation distances, respectively. Instead of choosing separation distances between every spacecraft pair, it is sometimes simpler to choose a separation distance between a spacecraft and a reference spacecraft. In this case, equation (2.3) can be replaced by

$$d_l^j \le d(\mathbf{y}, \mathbf{x}^j) \le d_u^j \qquad \forall \tau \tag{2.4}$$

where $\mathbf{y}$ is the state of the reference spacecraft. From these fundamentals, a family of formations can be defined as follows. If $d(\mathbf{y}, \mathbf{x}^j)$ is a constant for all j, then the formation is a *circular formation*,

$$d(\mathbf{y}, \mathbf{x}^j) = d_l^j = d_u^j \qquad \forall \tau \tag{2.5}$$

with the spacecraft at reference point $\mathbf{y}$ called the "mother" and the remaining j spacecraft denoted as "daughters". A circular formation can be defined even in the absence of a mother spacecraft. Thus, the mother spacecraft may be replaced by a

reference point, **y**, which serves the purpose of providing a non-inertial reference frame to the entire formation. *Multiple rings* of circular formations can similarly be defined with multiple distance bounds on a collection of spacecraft with respect to a single reference point.

A formation is defined to be *fully periodic* if the entire state vector is periodic,

$$\mathbf{x}^i(\tau_0) = \mathbf{x}^i(\tau_f) \tag{2.6}$$

and *partially periodic* if only some of the components of the state vector are periodic. For example, a formation may be partially periodic because it is periodic in position but not in velocity, or vice versa. If propellant is used to maintain a formation, then by this definition, the formation is partially periodic if the aperiodic mass is included as a state variable. It is apparent that a circular formation is a periodic formation but the reverse is not necessarily true. Of special note is that this definition for periodic motion can be either inertial or relative. Hence, periodicity in the relative frame does not necessarily imply periodicity in the inertial frame. That is, the swarm may drift in inertial space, but it will stay cohesive as a formation.

For a fully periodic formation using Cartesian position and velocity vectors as the state, the periodicity constraint may be written as,

$$\mathbf{r}(\tau_0) = \mathbf{r}(\tau_f) \tag{2.7}$$

$$\dot{\mathbf{r}}(\tau_0) = \dot{\mathbf{r}}(\tau_f) \tag{2.8}$$

These conditions allows us to further define two classes of partially periodic problems: (1) when only equation (2.7) is imposed while the boundary conditions on $\dot{\mathbf{r}}$ are free and (2) when only equation (2.8) is imposed while the boundary conditions on **r** are free. This thesis will limit its attention to fully periodic solutions and the two classes of partially periodic formations described above.

Finally, it must be noted that a formation need not be periodic at all! Hence, a *relaxed formation* is defined as the case when the state vector returns to within a defined space around the initial state after some time τ_f,

$$\boldsymbol{\varepsilon}_l \le \mathbf{x}_0^i - \mathbf{x}_f^i \le \boldsymbol{\varepsilon}_u \tag{2.9}$$

Thus, the familiar notion of an epsilon ball,

$$\left|\mathbf{x}_0^i - \mathbf{x}_f^i\right| \le \boldsymbol{\varepsilon} \tag{2.10}$$

is included in this definition.

The configuration is considered to be *optimal* if, in addition to satisfying the configuration constraint, a scalar performance measure,

$$J[\mathbf{x}(\cdot),\mathbf{u}(\cdot),\tau_0,\tau_f;\mathbf{p}] = \frac{1}{\tau_f - \tau_0}\int_{\tau_0}^{\tau_f} F(\mathbf{x}(\tau),\mathbf{u}(\tau),\tau;\mathbf{p})d\tau \tag{2.11}$$

is minimal. The reason for choosing a cost functional borrowed from optimal periodic control theory is that orbital motion is, by nature, periodic. Further, in addition to finding minimal fuel configurations, it is also desirable to find the *optimal period*, $\left[\tau_f - \tau_0\right]$ that renders a minimal cost per period.

To complete the optimal periodic control formalism,[14] the configuration constraints described in equation (2.1) are broken down into event constraints and path constraints. Event constraints are end point boundaries defined by

$$\mathbf{e}_l \le \mathbf{e}\left(\mathbf{x}^i(\tau_0),\mathbf{x}^i(\tau_f),\tau_0,\tau_f\right) \le \mathbf{e}_u \tag{2.12}$$

Path constraints are boundaries placed on the trajectory of the model,

$$\mathbf{g}_l \le \mathbf{g}\left(\mathbf{x}^i(\tau),\mathbf{u}^i(\tau),\tau\right) \le \mathbf{g}_u \tag{2.13}$$

Additionally, each of the state and control variables may have a constraint placed on them by

$$\mathbf{x}_l^i \le \mathbf{x}^i(\tau) \le \mathbf{x}_u^i \tag{2.14}$$

$$\mathbf{u}_l^i \le \mathbf{u}^i(\tau) \le \mathbf{u}_u^i \tag{2.15}$$

All of the constraints shown above can be used as equality constraints by simply setting the upper and lower bounds equal. They are written as inequalities for the purpose of generality. Any formation configuration may now be defined in this "standard" form as finding the controls, $\mathbf{u}^i(\tau)$, and the optimal period, $\left[\tau_f - \tau_0\right]$, that minimize the cost of equation (2.11).

1. Reference Frame

In order to describe relative position, motion, and configurations, the Formation Reference Frame will be used throughout this thesis. Figure II-1 shows this reference frame, which is defined with $\hat{x}$ pointing in the radial direction, $\hat{y}$ pointing perpendicular to $\hat{x}$ along the direction of motion, and $\hat{z}$ completing the right-handed coordinate system. This reference frame is often called RSW or Satellite Coordinate System.[20]

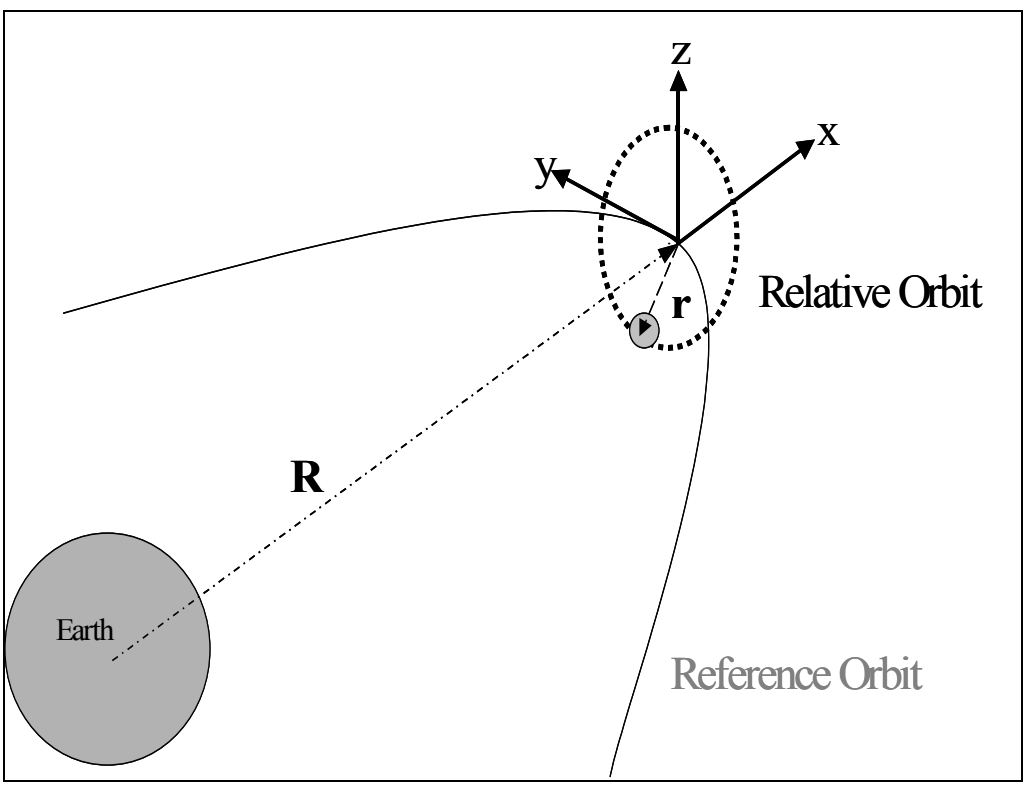

Figure II-1 Formation Reference Frame

The assumption of the coordinate system is important in defining any problem. For some coordinate systems, the formation relative motion and configuration constraints are intuitive. For example, the path constraint for a circular formation can be described in the formation reference frame simply using the relative position

$$r_x^2 + r_y^2 + r_z^2 = constant \tag{2.16}$$

On the other hand, to describe this constraint in the inertial frame requires a transformation to that frame. This transformation need only be completed once, but can be very labor intensive.

This same concern must be applied to the dynamic equations of motion. The complete, non-linear equations can be readily expressed, with no assumptions, in the inertial frame by

$$\ddot{\mathbf{R}}^N = -\mu \frac{\mathbf{R}}{|\mathbf{R}|^3} + \mathbf{a}^N_{perturbations} \tag{2.17}$$

Conversely, in the formation reference frame a transformation is again required and usually involves introducing assumptions and linearizations.

Equal to the coordinate system in importance is the choice of the variables used to describe the satellite state. One set of variables is the Cartesian position and velocity vectors. Other sets available include many different orbital element sets, which are especially useful if the coordinate system is Earth centered and inertial. However, if the solution calls for control thrusting, it will be a complex translation into the orbital elements. For these and other reasons, all models presented in this thesis utilize Cartesian position and velocity vectors in the Formation Reference Frame as the basic spacecraft state. Depending on the model, there may be additional variables in the state, but there will be a minimum of these six.

B. SOLVING OPTIMAL CONTROL PROBLEMS

Until recently, solving general nonlinear optimal control problems was an arduous or impossible task. The theoretical framework for solving such problems is the Minimum Principle.[21] Numerical methods based on the Minimum Principle are known as indirect

methods.[22] While solutions obtained from indirect methods are accurate in the sense that they satisfy the necessary conditions of optimality, they are fundamentally burdened by numerical sensitivities as noted by Kalman over four decades ago.[23] The so-called indirect multiple shooting methods and indirect collocation methods overcome this computational instability problem but at the expense of convergence: good guesses on the costate time-history are necessary to successfully solve the problem. Over the last decade, the so-called direct methods have come to the forefront. These methods bypass the Minimum Principle and "directly" solve the problem in various ways. Betts provides an excellent review of this approach.[22] Early direct methods were plagued by inaccuracies, particularly in the determination of the controls. More recently, major breakthroughs in higher-order methods and large sparse numerical methods have quickly narrowed this gap.[12] One particular approach is to use a solution obtained from a direct method as a guess for an indirect method. Another approach, favored in this thesis, is called the Legendre pseudospectral method.[12] This method is used to solve the formation design and control problems posed and is implemented in the reusable software package, DIDO. Unless otherwise specified, all results reported in this thesis are obtained using this software.

1. Necessary Conditions for Optimality*

The first step in solving an optimal control problem is to construct a scalar function called the Hamiltonian, H,

$$H\left(\mathbf{x},\mathbf{u},t,\boldsymbol{\lambda}\right)=\frac{F\left(\mathbf{x},\mathbf{u},t\right)}{\tau_f-\tau_0}+\boldsymbol{\lambda}\left(t\right)^{\mathrm{T}}\mathbf{f}\left(\mathbf{x},\mathbf{u},t\right) \tag{2.18}$$

where $\mathbf{f}\left(\mathbf{x},\mathbf{u},t\right)$ are the dynamic constraints on the system, and $\boldsymbol{\lambda}\left(t\right)$ are the Lagrange multipliers called costates. According to the Minimum Principle, at each instant of time, the optimal control is obtained by solving the following problem.

Minimize H with respect to $\mathbf{u}$, with $\mathbf{u}\in U$

* Most of the information in this section comes from class notes and discussion from AA 4850 and is reproduced here for completeness.

where U is the set of all allowable controls. To solve this problem, the Lagrangian of the Hamiltonian must be constructed:

$$L(\mathbf{x},\mathbf{u},t,\boldsymbol{\lambda},\boldsymbol{\phi}) = H(\mathbf{x},\mathbf{u},t,\boldsymbol{\lambda}) + \boldsymbol{\phi}(t)^{\mathrm{T}}\,\mathbf{g}(\mathbf{x},\mathbf{u},t) \tag{2.19}$$

where $\mathbf{g}(\mathbf{x},\mathbf{u},t)$ are the path constraints and $\boldsymbol{\phi}(t)$ are the associated Lagrange multipliers. The path constraints include all trajectory path constraints as well as any state and control bounds. Applying the Karush-Kuhn-Tucker (KKT) theorem to the Lagrangian results in a set of necessary conditions and provides a means to demonstrate the optimality of a solution.

$$\frac{\partial L}{\partial \mathbf{u}} = \mathbf{0} \tag{2.20}$$

$$\boldsymbol{\phi}(t)^{\mathrm{T}}\,\mathbf{g}(\mathbf{x},\mathbf{u},t) = \mathbf{0} \tag{2.21}$$

with

$$\boldsymbol{\phi} = \begin{cases} \leq 0 & \\ \geq 0 & \\ = 0 & \\ any & \end{cases} \quad if \quad \begin{array}{l} g_l = g(\mathbf{x},\mathbf{u},\tau) \\ g(\mathbf{x},\mathbf{u},\tau) = g_u \\ g_l < g(\mathbf{x},\mathbf{u},\tau) < g_u \\ g_l = g_u \end{array} \quad term\ by\ term \tag{2.22}$$

The third case above describes a special condition when the constraints in $\mathbf{g}$ are interior or non-binding,

$$\mathbf{g}_l < \mathbf{g}(\mathbf{x},\mathbf{u},t) < \mathbf{g}_u \tag{2.23}$$

For these cases, the multipliers, $\boldsymbol{\phi} = \mathbf{0}$ and equation (2.20) simplifies to

$$\frac{\partial L}{\partial \mathbf{u}} = \frac{\partial H}{\partial \mathbf{u}} = \mathbf{0} \tag{2.24}$$

It is desirable to have interior constraints because the problem behaves as if the constraints do not exist. For this reason, the constraints placed on a problem may have an actual value in practice, but if sufficiently large as to be non-binding, they can be described as unconstrained.

2. Scaling

Scaling is critical to all optimal control problems. The goal is to establish a scheme that scales all parameters and state variables so that they are close to one another in value. For example, it is better to have positions from 0-10 with velocities from 1-10 than positions from 7000-17000 with velocities from 0-10. The method for scaling the problem starts with setting a desired unit and determining the remaining units that comply with this standard. For the problems that follow, the desired standard unit was time. The time unit was chosen to go from 0 to 1 for a single orbital period. The normalization constant, TU, is defined to be equal to the period of the reference orbit in seconds. This can be done several ways, but the most simple way is to select a value for the semi-major axis, a, and use the following equation

$$TU = 2\pi\sqrt{\frac{a^3}{\mu}} \tag{2.25}$$

where μ is the gravitational parameter of the earth and is set to

$$\mu = 3.986004418\text{x}10^{14}\ \frac{\text{m}^3}{\text{s}^2} \tag{2.26}$$

The normalized time now becomes

$$\tau_{nondim} = \frac{\tau}{TU} \tag{2.27}$$

and therefore, the orbital period becomes 1.0 TU. This definition for the time unit, by nature, defines the mean motion since

$$n_{nondim} = \frac{2\pi}{Orbital\ \ Period} = 2\pi/TU \tag{2.28}$$

The next variable to be selected is the mass unit, MU, which is simply chosen to be equal to the initial mass of the spacecraft or

$$m_{0_{nondim}} = \frac{m_0}{MU} = 1.0 \tag{2.29}$$

The last variable that is chosen by the user is the standard distance unit, RU. The choice for this unit is based on the desired formation spacing. It can be varied to provide larger or smaller formations without affecting the configuration. Given TU and RU, the remaining variables can be normalized as follows

$$\mathbf{r}_{nondim} = \frac{\mathbf{r}}{RU} \tag{2.30}$$

$$\dot{\mathbf{r}}_{nondim} = \frac{\dot{\mathbf{r}}}{RU/TU} \tag{2.31}$$

$$\mathbf{a}_{p_{nondim}} = \frac{\mathbf{a}_p}{RU/TU^2} \tag{2.32}$$

Unless dimensional units are specified, all values are assumed to be scaled and nondimensional and the *nondim* subscript will be dropped.

3. Unique Issues for Periodic Problems

As with any optimization problem, most errors are not in the solution but in asking the right question. One special issue with periodic optimization problems is formulating an initial guess. Every optimizer requires a first guess, whether it is provided by the user or calculated by the solver. The quality of the guess is often an issue, as some solvers require relatively accurate guess. DIDO does not require a good quality guess or even a feasible guess. However, a simple linear interpolation between the endpoints is not an option for periodic problems. The explanation lies in the periodicity condition itself. For orbits, even a straight line cannot be used as a guess since the motion is elliptical in nature. Some sort of ellipse must be used as a guess for orbital motion.

Determining the cost function is another difficult part of configuration design. It affects not only the speed of the solution, but the solution itself. For example, beginning with section III.D, thrust and mass are used in the non-linear equations of motion. The cost function can be written simply as

$$J = \frac{m_f - m_0}{\tau_f - \tau_0} \tag{2.33}$$

On the other hand, it can also be written as

$$J = \frac{1}{\tau_f - \tau_0} \int_{\tau_0}^{\tau_f} |T_x| + |T_y| + |T_z| \, d\tau \tag{2.34}$$

which also results in a minimum mass expended. It turns out that for zero or very low thrust problems the change in mass is very small and may be below the numeric tolerance of the solver. This often results in a sub-optimal solution. When thrust is used in the cost, since it is a control variable, the solver is better able to find the optimal solution.

Another aspect that proved interesting was the $(\tau_f - \tau_0)$ term, used to represent the optimal period. For Natural or Zero-Thrust solutions, the optimal period was exactly equal to the orbital period. However, once thrust is required to maintain the formation the optimal period may or may not equal the orbital period. One way to get around this disparity is to force the solution period to be equal to the orbital period, that is $t_f = 1.0$.

C. VALIDATING SOLUTIONS

The purpose of this section is to describe the various methods used to validate the numerical solutions. Numerical methods may seem to discard the physics of the problem and rely solely on the mathematics, but this is far from the truth. Any solution found numerically must be 'assessed' to see if it is in fact a feasible and legitimate solution. It is precisely here that the "Physics" intuition and knowledge are implemented to assist in verification. To that end, there are many different ways to verify that a solution is feasible. The optimality of a solution can be demonstrated using the optimality conditions described in section B.1. Each of the three primary means of validating solutions are described below.

1. Numeric Propagators

The primary method for validating feasibility of the solutions is to propagate them using a numerical propagator. Since the equations of motion are Ordinary Differential Equations (ODE), a tool is needed to solve them for each desired time step. The environment for DIDO is MATLAB®, so a resident ODE solver was used. There are

several to choose from, but ODE45 is the most common and usually the most capable for non-stiff equations.

The first step in validating is to build a propagator from the ODE solver. This requires defining the Equations of Motion (EOM) that govern the behavior for the solver and establishing the initial conditions. The initial conditions were taken directly from the DIDO solution. It is important for the EOM to be the same as the ones used to find the solution, to ensure an accurate validation under the same assumptions. It does no good to make assumptions in defining the problem, only to forget about them in validating the results.

2. Commercial Software

Another method employed to validate solutions is the use of commercial software. Both Satellite Tool Kit® (STK), from Analytical Graphics, Inc. and FreeFlyer®, from A.I. Solutions were used as an independent source for propagating the formations. Usually these programs are used for visualization and presentation, but both software suites include a very robust non-linear propagator. Any number of reports can be selected to identify and track the desired parameters. Each of the programs also includes a viewing capability that allows the user to be placed on the reference point observing the formation from that perspective. This directly corresponds to the Formation Reference Frame shown in Figure II-1 and is very useful in visualizing relative formations.

The mechanism for validating solutions using these programs is to import the *initial conditions* for the individual formation satellites into the programs and propagate them forward. This can be done directly from MATLAB for use in FreeFlyer, or with an Ephemeris file for use in STK. If the solution requires active control, then the control history must also be imported into the programs. Other than initial conditions and/or controls, there is no other information provided to the software. This lack of information is exactly what validates the solutions. If the formation behaves as predicted in the solution when propagated by the software, then the formation is feasible.

3. Previously Discovered Solutions

The third method is used to validate the method more than it is to validate a particular solution. If the method is employed and is able to identify previously discovered solutions, it is valid. The ultimate validation would be to demonstrate that this method is able to find all previously discovered solutions. Rather than devote precious time to an exhaustive catalog of all prior solutions to all satellite formations, several representative formations were chosen as demonstrations of the ability. Specifically, the well-known circular and projected circular solutions to the Hill-Clohessy-Wiltshire equations were reproduced. For an example using elliptical reference orbits, Reference 17 outlines a solution with $e = 0.7$ for the reference satellite.

III. CIRCULAR REFERENCE ORBIT

A. PROBLEM DEFINITION

The framework described in the previous chapter can be applied to designing and controlling spacecraft formations subject to any arbitrary forces. This chapter begins by applying this framework to spacecraft subject to an inverse-square gravity field only. If the equations of motion are linearized in the formation reference frame about a circular reference orbit, the C-W equations are obtained and closed-form solutions are easily found. From these equations, it is apparent that zero-propellant formations exist making this problem an excellent starting point. These equations also served as a good model with which to validate the process for this class of periodic problems.

One zero-propellant solution to the C-W equations is a circular formation. In order to solve this problem the following configuration was used. The state consists of the Cartesian relative position and velocity components shown below

$$\mathbf{x} = \begin{bmatrix} \mathbf{r}^{\mathrm{T}} & \dot{\mathbf{r}}^{\mathrm{T}} \end{bmatrix}^{\mathrm{T}} = \begin{bmatrix} r_x & r_y & r_z & \dot{r}_x & \dot{r}_y & \dot{r}_z \end{bmatrix}^{\mathrm{T}} \tag{3.1}$$

The state constraints were

$$\begin{aligned} -2r \le r_x, r_y, r_z \le 2r \\ -\dot{r}_{max} \le \dot{r}_x, \dot{r}_y, \dot{r}_z \le \dot{r}_{max} \end{aligned} \tag{3.2}$$

where $\dot{r}_{max}$ was chosen arbitrarily. The position constraints, while specified, were never active due to a tighter path constraint. The velocity constraints were not active either due to the choice of $\dot{r}_{max}$. The controls, representing the relative accelerations in each axis, were constrained by

$$-u_{max} \le u_x, u_y, u_z \le u_{max} \tag{3.3}$$

with u_{max} specified by the user. Since the solution is a zero control solution, these constraints were also inactive.

The event constraints were specified for a fully periodic solution using equations (2.7) and (2.8) although they were written in the form

$$\mathbf{x}(\tau_0) - \mathbf{x}(\tau_f) = 0 \tag{3.4}$$

or more specifically

$$\begin{bmatrix} r_x(\tau_0) \\ r_y(\tau_0) \\ r_z(\tau_0) \\ \dot{r}_x(\tau_0) \\ \dot{r}_y(\tau_0) \\ \dot{r}_z(\tau_0) \end{bmatrix} - \begin{bmatrix} r_x(\tau_f) \\ r_y(\tau_f) \\ r_z(\tau_f) \\ \dot{r}_x(\tau_f) \\ \dot{r}_y(\tau_f) \\ \dot{r}_z(\tau_f) \end{bmatrix} = \begin{bmatrix} 0 \\ 0 \\ 0 \\ 0 \\ 0 \\ 0 \end{bmatrix} \tag{3.5}$$

The path constraint, $\mathbf{g}$, for a circular formation is defined by

$$(r-\delta)^2 \le \left(r_x^2 + r_y^2 + r_z^2\right) \le (r+\delta)^2 \tag{3.6}$$

This general form of the path constraint includes an allowance for a tolerance, which for circular formations is set to zero or for near-circular formations is nonzero. For this case, the path constraint for a circular formation and the event constraint for a fully periodic formation are redundant. The path constraint will force a fully periodic solution, even in the absence of any event constraints. This was demonstrated and validated during several of the solution sets.

The cost function to be minimized was

$$J = \frac{1}{\tau_f - \tau_0} \int_{\tau_0}^{\tau_f} \left(u_x^2 + u_y^2 + u_z^2\right) d\tau \tag{3.7}$$

which is identical to a cost that was based on the absolute value of each control acceleration, if the solution is a zero-control solution.

B. EQUATIONS OF MOTION

Since the equations of motion for this model are well known[15,24,25,26] their derivation will not be described here. Instead, only the equations and their assumptions will be presented.

$$\ddot{\mathbf{r}} = \begin{bmatrix} 0 & 2n & 0 \\ -2n & 0 & 0 \\ 0 & 0 & 0 \end{bmatrix} \dot{\mathbf{r}} + \begin{bmatrix} 3n^2 & 0 & 0 \\ 0 & 0 & 0 \\ 0 & 0 & -n^2 \end{bmatrix} \mathbf{r} + \begin{bmatrix} u_x \\ u_y \\ u_z \end{bmatrix} \tag{3.8}$$

where $\mathbf{r}$ is the vector representing the inter-satellite distance expressed in the formation reference frame (see Figure II-1),

$$\mathbf{r} = \begin{bmatrix} \hat{x} & \hat{y} & \hat{z} \end{bmatrix}^T \tag{3.9}$$

or in state form:

$$\dot{\mathbf{x}} = \begin{bmatrix} 0 & 0 & 0 & 1 & 0 & 0 \\ 0 & 0 & 0 & 0 & 1 & 0 \\ 0 & 0 & 0 & 0 & 0 & 1 \\ 3n^2 & 0 & 0 & 0 & 2n & 0 \\ 0 & 0 & 0 & -2n & 0 & 0 \\ 0 & 0 & -n^2 & 0 & 0 & 0 \end{bmatrix} \mathbf{x} + \begin{bmatrix} 0 \\ 0 \\ 0 \\ u_x \\ u_y \\ u_z \end{bmatrix} \tag{3.10}$$

Two of the primary assumptions of this model are a spherical earth with no other perturbing forces present and a circular reference orbit. Both of these assumptions lead to unstable formations when applied to actual orbits since their effects are significant. The latter assumption is the primary focus of this thesis and will be addressed in a later chapter. The third assumption is

$$r \ll R \tag{3.11}$$

which remains valid for most formations even when applied to actual orbits.

C. C-W SOLUTIONS

For all solutions shown in this thesis, the filled circles show the node points corresponding to the solution. They vary in number based on an arbitrary user-defined specification. The nature of the solver is such that the spacing between node points is not

constant. Instead, the points are closer together at the endpoints than they are in the middle. The solid lines represent the motion of the *propagated* initial conditions. The **solutions for the C-W equations of motion are not shown** for the sake of brevity since they are identical, within numeric tolerances, to the solutions for the new equations shown later.

1. C-W Circular Solution

For the C-W equations, imposing the condition of full periodicity and restricting the inter-satellite range to a constant distance from the center X (at point [0,0,0]) produces a circular satellite formation.

The final time for the optimal period was not fixed. The solution was not only able to determine the optimal trajectory, but also the optimal period in which to complete its trajectory. As expected, the solution resulted in $\tau_f = 1.0$, meaning the optimal period was exactly equal to one orbital period. Interestingly, when asked to find a solution over 2 orbits, the same 1-orbit solution was found, only it was now shown over the 2 orbits.

2. C-W Projected Circular Solution

Another well-known solution to the C-W equations is the projected circular formation.[26] This solution maintains the appearance of a circular formation as seen from the surface of the earth, but is in fact elliptical. To accomplish this formation a different path constraint, $\mathbf{g}$, was imposed.

$$(r-\delta)^2 \le \left(r_y^2 + r_z^2\right) \le (r+\delta)^2 \tag{3.12}$$

It is no longer the three dimensional range that was constrained but the range from the reference point to the satellite in a certain plane, namely the cross-track versus along-track plane. As with the circular formation, the optimal period was not fixed, and again it was exactly equal to the orbital period.

D. NON-LINEAR TWIST

To further amplify the notion that *linear models are not necessary for this approach*, Thrust was chosen as a control variable instead of acceleration. Not only is this more realistic but it also makes the "linear" equations "nonlinear" due to a non-zero

mass flow rate. This requires the addition of Mass as one of the state variables, in addition to the relative position and velocity components.

$$\mathbf{x} = \begin{bmatrix} r_x & r_y & r_z & \dot{r}_x & \dot{r}_y & \dot{r}_z & m \end{bmatrix}^{\mathrm{T}} \tag{3.13}$$

The path constraint remains the same as equations (3.6) or (3.12). The state constraints now include the following constraint on mass:

$$0.10 \le m(\tau) \le 1.0 \tag{3.14}$$

which assumes a minimum mass of 10 percent of the original mass and a maximum mass equal to the original mass. The event constraints also contain the new event

$$m(\tau_0) = 1.0 \tag{3.15}$$

to force a starting mass at the beginning of the solution.

The controls represent thrust in a given axis and are constrained by

$$-T_{max} \le T_x, T_y, T_z \le T_{max} \tag{3.16}$$

with T_{max} usually chosen in such a way as to make the constraint inactive. The desired cost is the total amount of thrust expended and can be described as

$$J = \frac{1}{\tau_f - \tau_0} \int_{\tau_0}^{\tau_f} |T_x| + |T_y| + |T_z| \, d\tau \tag{3.17}$$

but was implemented as

$$J = \frac{1}{\tau_f - \tau_0} \int_{\tau_0}^{\tau_f} \left(T_x^2 + T_y^2 + T_z^2 \right) d\tau \tag{3.18}$$

This cost function could have been implemented as seen in equation (3.17) but, for numerical performance reasons, equation (3.18) was chosen. If the cost in equation (3.17) is minimized, the formation solution will be identical to the formation found by minimizing the cost in equation (3.18), when $T_i = 0$. For zero-thrust solutions, the main difference is the speed of the process.

1. New Equations of Motion

The equations of motion for this case are similar to Equation (3.8) except the control accelerations, $\mathbf{u}$, are replaced with thrust.

$$\ddot{\mathbf{r}} = \begin{bmatrix} 0 & 2n & 0 \\ -2n & 0 & 0 \\ 0 & 0 & 0 \end{bmatrix} \dot{\mathbf{r}} + \begin{bmatrix} 3n^2 & 0 & 0 \\ 0 & 0 & 0 \\ 0 & 0 & -n^2 \end{bmatrix} \mathbf{r} + \frac{1}{m} \begin{bmatrix} T_x \\ T_y \\ T_z \end{bmatrix} \tag{3.19}$$

Another equation must be included to govern the new state variable of mass. This mass flow rate is

$$\dot{m} = \frac{-T}{v_e} \tag{3.20}$$

Note that T is not the magnitude of the thrust vector, but is defined as $T = |T_x| + |T_y| + |T_z|$ and v_e is the characteristic exhaust velocity of the thruster.

2. Circular Formation Solution with New EOM

The circular formation solutions to the new EOM are obtained using the path constraint shown in equation (3.6). Table III-1 shows the constraints used for this solution. Figure III-1 shows the three-dimensional view, while Figure III-2 to Figure III-4 show the orthogonal projections. Figure III-3 also shows the planar motion in the $\hat{x} - \hat{z}$ plane at an angle of 60° to greater than 10^{-9} accuracy. Figure III-5 shows the thrust profile, which is equal to zero-thrust within numerical tolerances.

Table III-1 Constraints for Circular Formation

Constraint	***Normalized Lower and Upper Bounds***
States: r_x, r_y, r_z	Unconstrained
States: $\dot{r}_x, \dot{r}_y, \dot{r}_z$	Unconstrained
States: m	[0.1 : 1.0]
Controls: $\mathbf{T}$	Unconstrained
Time: τ	Unconstrained
Events: $\mathbf{r}(\tau_0) - \mathbf{r}(\tau_f)$	[0.0 : 0.0]
Events: $\dot{\mathbf{r}}(\tau_0) - \dot{\mathbf{r}}(\tau_f)$	[0.0 : 0.0]
Path: $g = r_x^2 + r_y^2 + r_z^2$	[1.0 : 1.0]
Number of Nodes	120
Reference Orbit: e	0.0

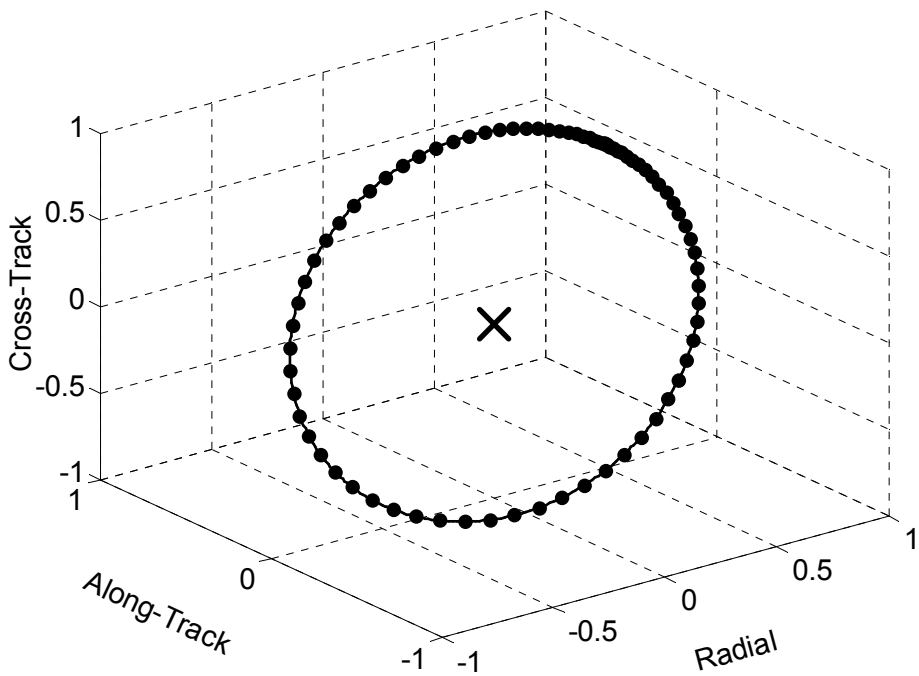

Figure III-1 Circular Formation Using New Equations of Motion

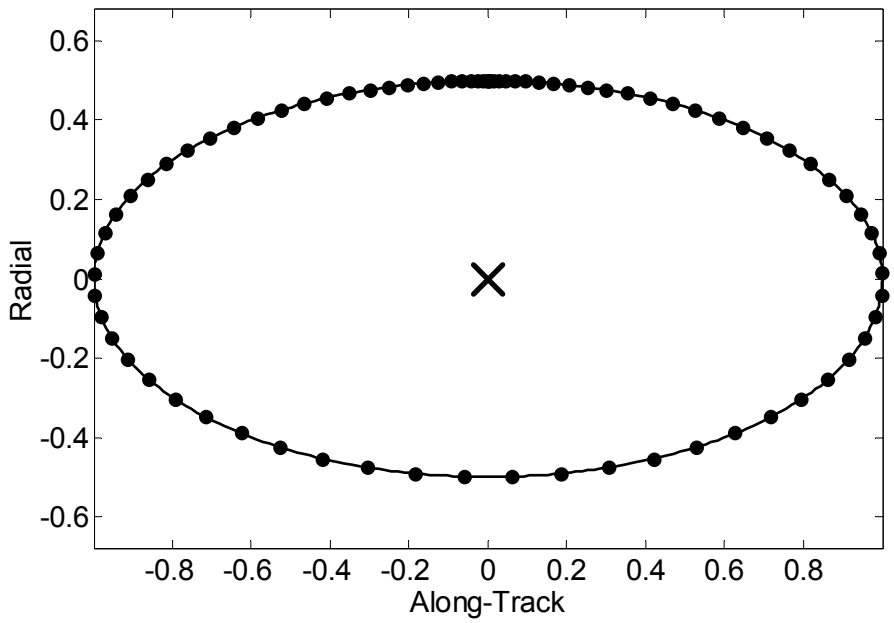

Figure III-2 Radial vs. Along-Track Motion for a Circular Formation

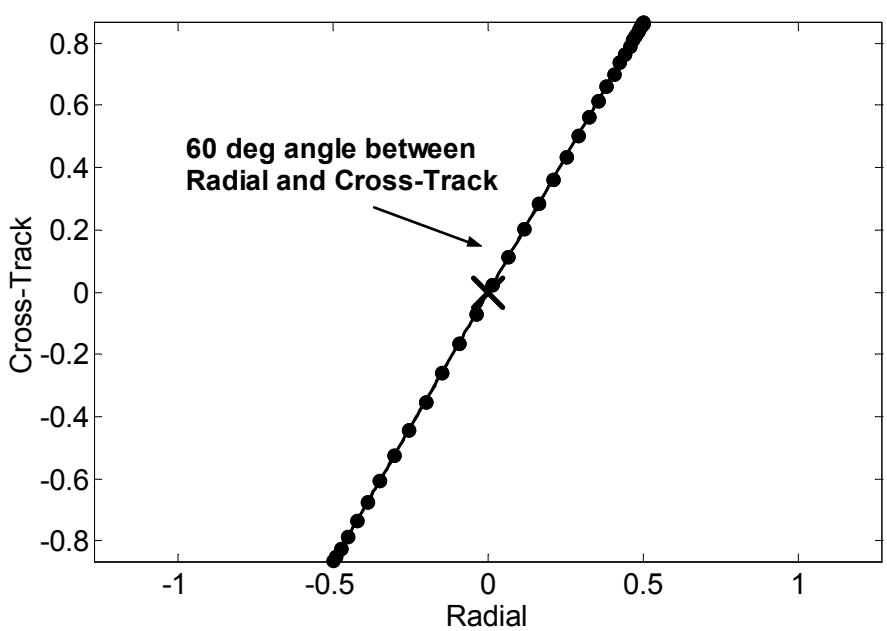

Figure III-3 Cross-Track vs. Radial Motion for a Circular Formation

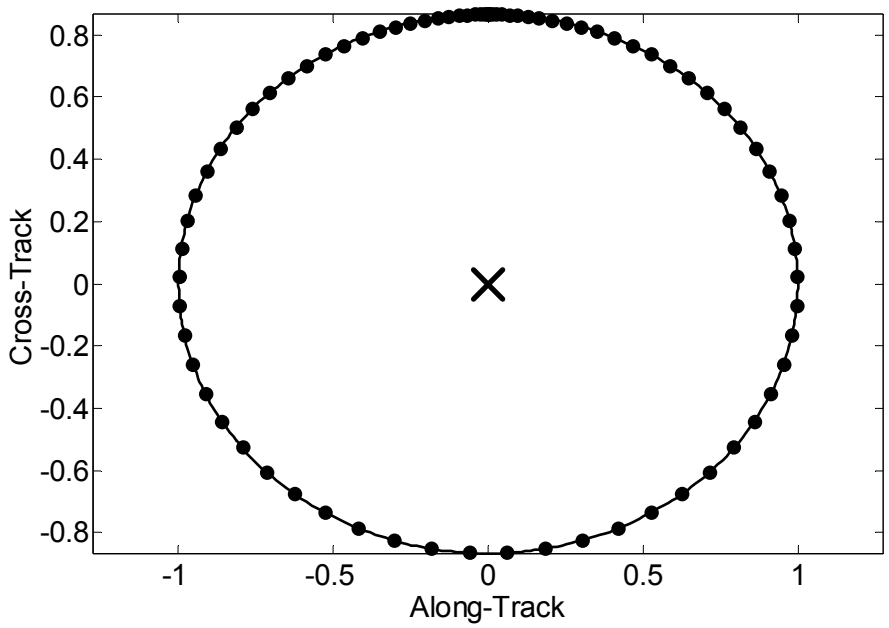

Figure III-4 Cross-Track vs. Along-Track Motion for a Circular Formation

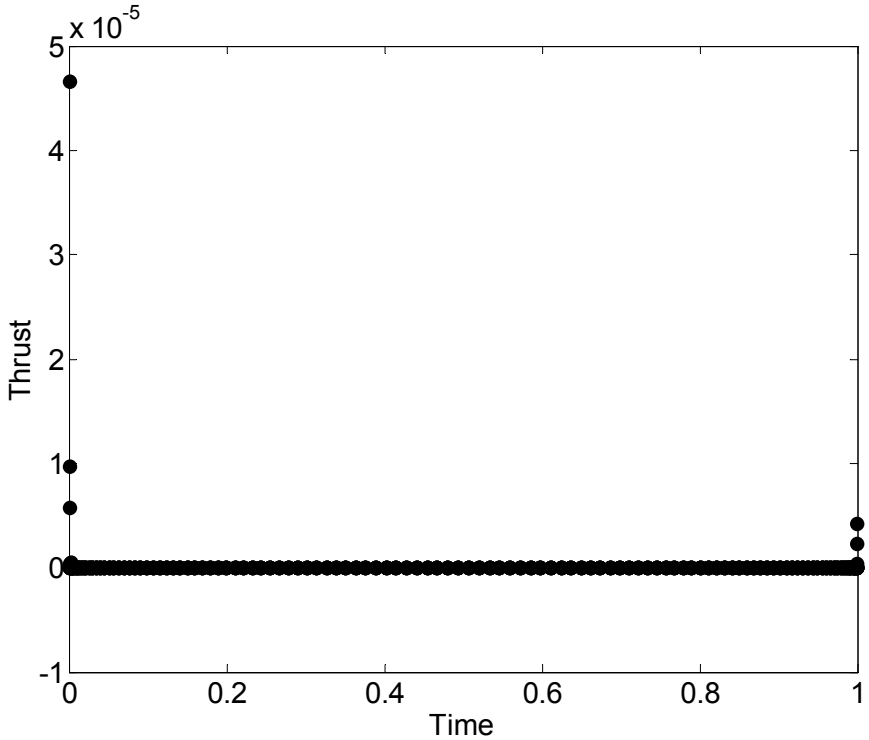

Figure III-5 Thrust Profile for Circular Formation with New EOM

3. Projected Circular Formation Solution with New EOM

The projected circular formation solutions utilize the new EOM with the path constraint in equation (3.12). Table III-2 shows the constraints while Figure III-6 shows the three-dimensional view. Figure III-7 to Figure III-9 show the orthogonal projections and Figure III-10 shows the thrust profile.

Table III-2 Constraints for Projected Circular Formation

Constraint	***Normalized Lower and Upper Bounds***
States: r_x, r_y, r_z	Unconstrained
States: $\dot{r}_x, \dot{r}_y, \dot{r}_z$	Unconstrained
States: m	[0.1 : 1.0]
Controls: $\mathbf{T}$	Unconstrained
Time: τ	Unconstrained
Events: $\mathbf{r}(\tau_0) - \mathbf{r}(\tau_f)$	[0.0 : 0.0]
Events: $\dot{\mathbf{r}}(\tau_0) - \dot{\mathbf{r}}(\tau_f)$	[0.0 : 0.0]
Path: $g = r_y^2 + r_z^2$	[1.0 : 1.0]
Number of Nodes	100
Reference Orbit: e	0.0

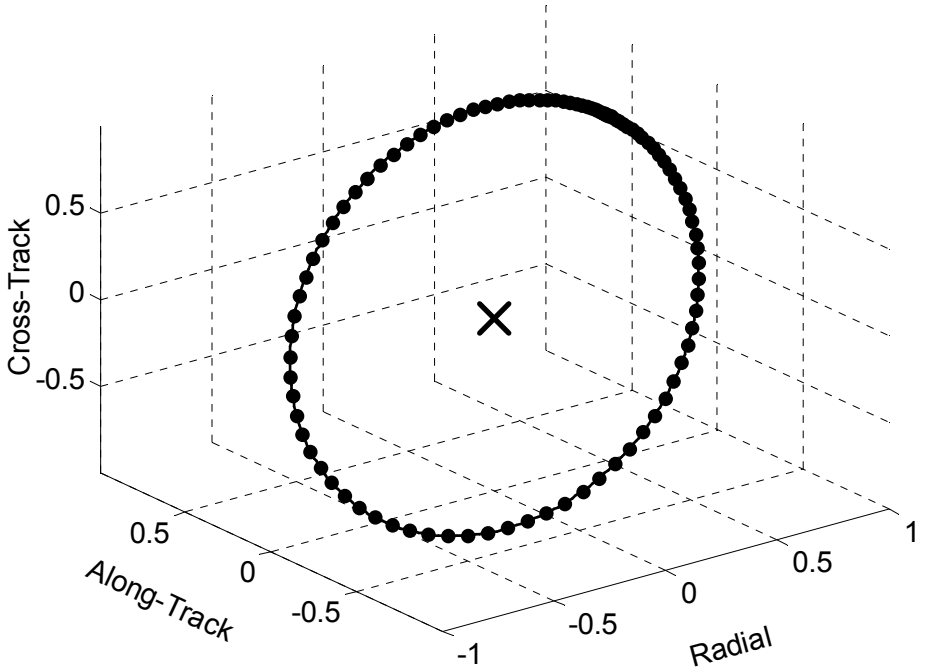

Figure III-6 Projected Circular Formation Using New Equations of Motion

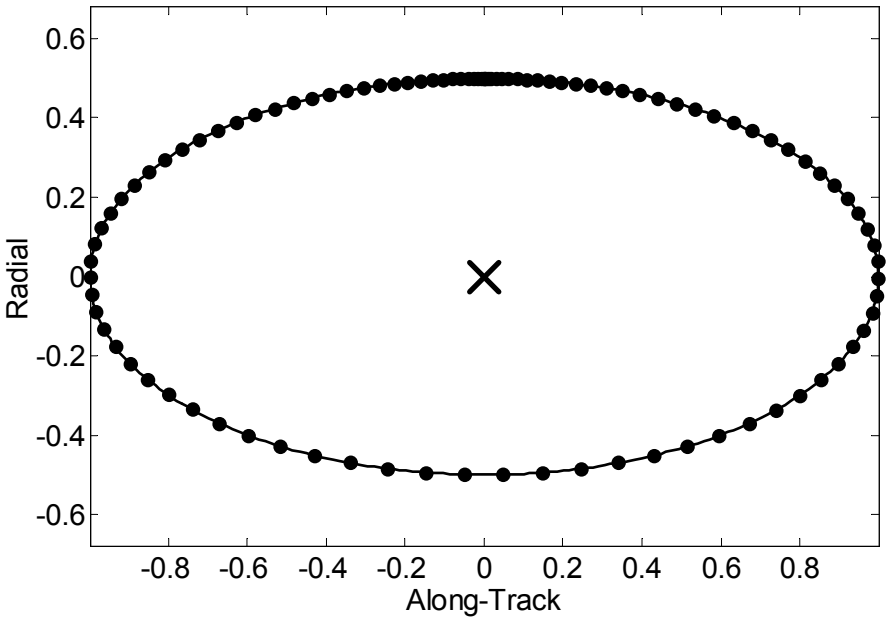

Figure III-7 Radial vs. Along-Track Motion for a Projected Circular Formation

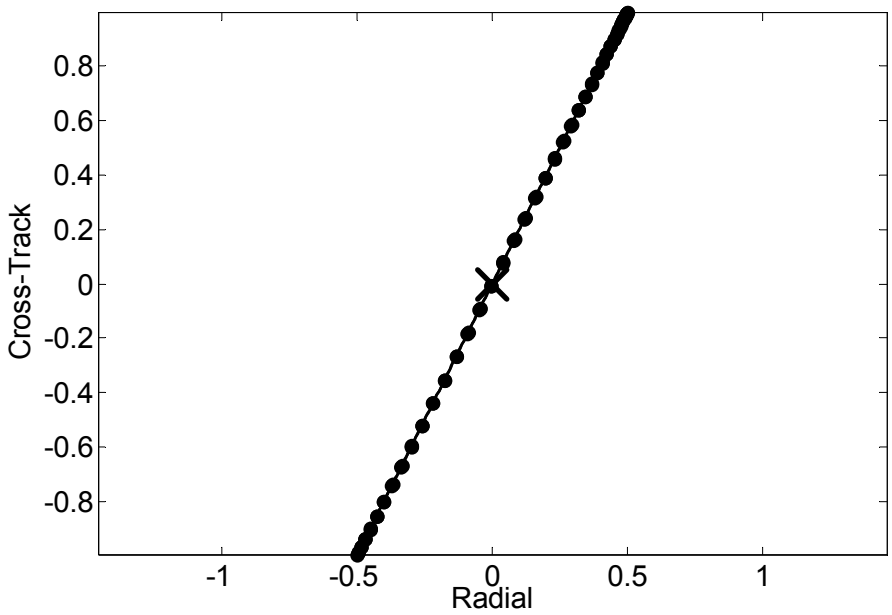

Figure III-8 Cross-Track vs. Radial Motion for a Projected Circular Formation

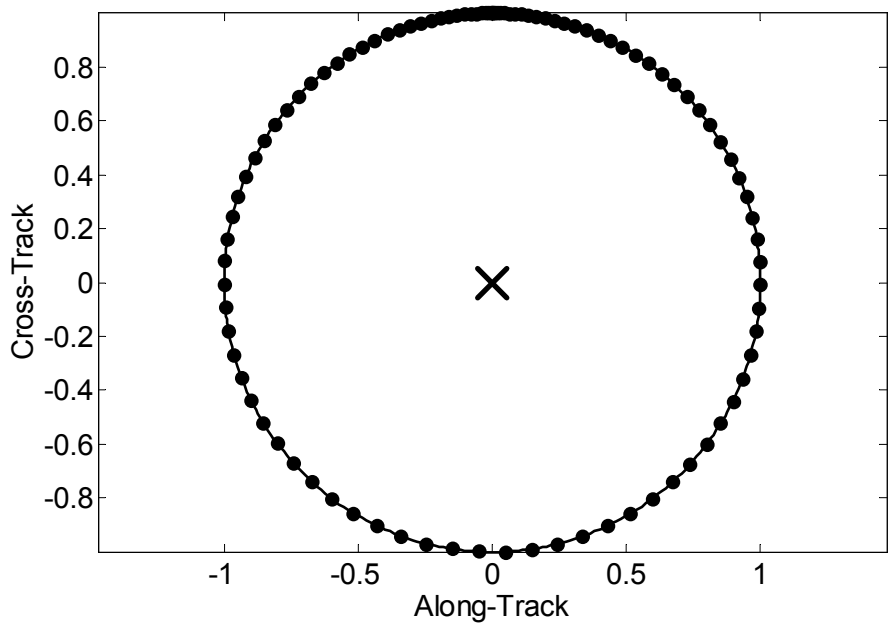

Figure III-9 Cross-Track vs. Along-Track Motion for a Projected Circular Formation

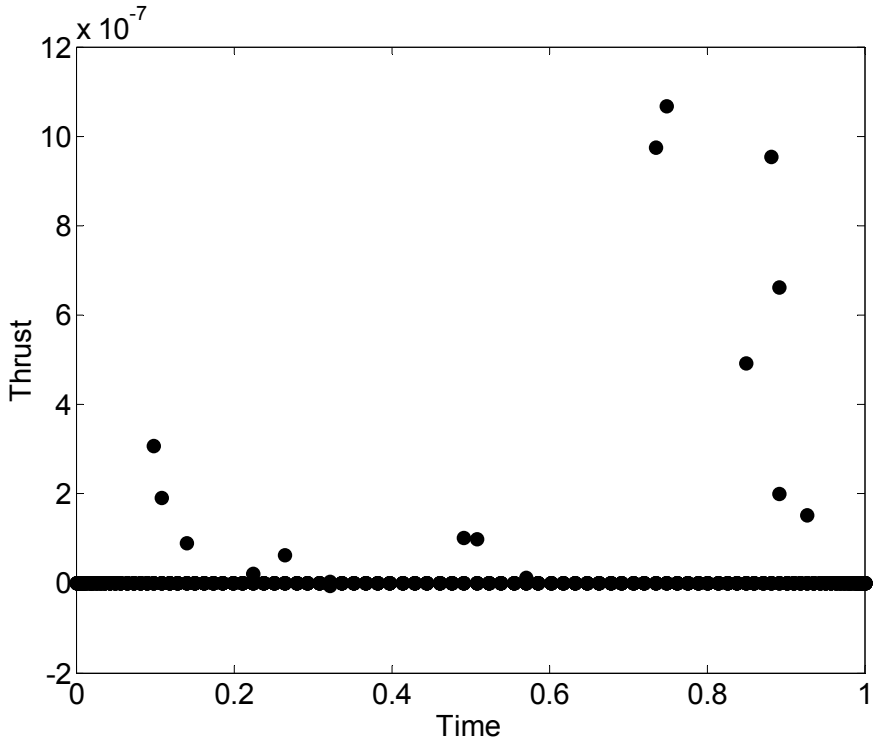

Figure III-10 Thrust Profile for Projected Circular Formation with New EOM

E. VALIDATION OF SOLUTIONS

Since the answer to these problems was known, the validation was simply to compare the numerical solution to the analytical solution. This was accomplished using Figure III-1 through Figure III-10 as well as unique characteristics such as the angle of the plane of relative motion seen in Figure III-3. This angle was calculated for each solution and verified against the known values.[25]

Validation was also accomplished by numerically propagating the initial conditions for a set number of orbits, arbitrarily chosen as 50 orbits and is shown in Figure III-11 and Figure III-12. Table III-3 shows the results from propagating the initial conditions of the *analytical solution*. Table III-4 and Table III-5 show the results for propagating the initial conditions from the DIDO solution for the circular formation and projected circular formation, respectively. The errors seen in Table III-3 form the baseline for interpreting the errors in every other solution propagation. The source of

these errors is the numeric propagator, since the equations of motion used to propagate are the same as the analytical model.

As mentioned previously, the optimal period was not fixed for these problems. Each of the solutions in this chapter yielded an optimal period equal to the orbital period, which was further verification of agreement with the known solutions.

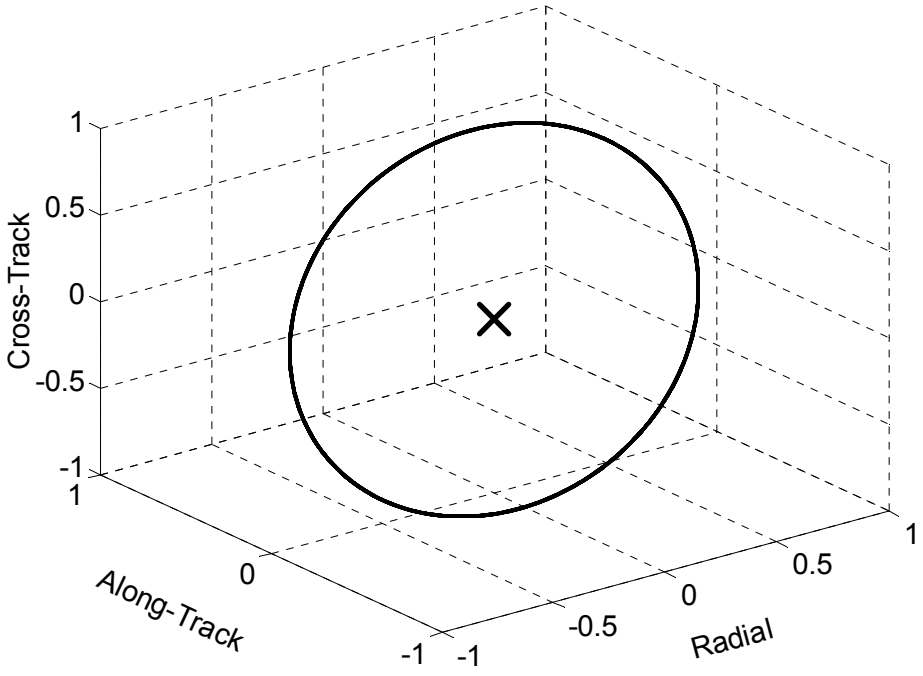

Figure III-11 Circular Solution Over 50 Orbits

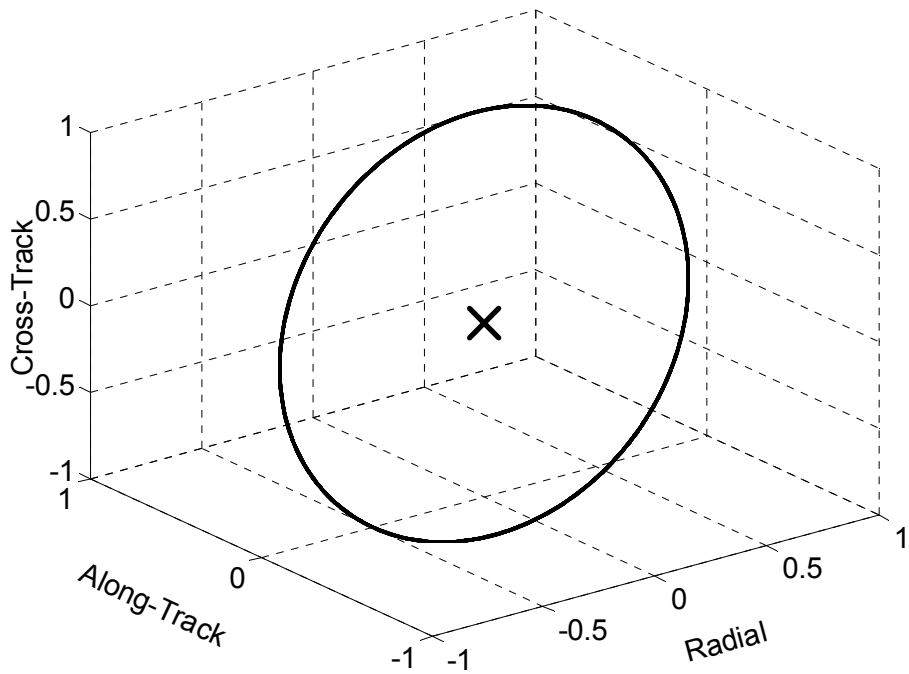

Figure III-12 Projected Circular Solution Over 50 Orbits

Table III-3 Propagation Results for Analytical C-W Circular Solution

State Variable	***% Difference Between Initial and Final Values***
r_x	9.84 x10^{-4}
r_y	1.33 x10^{-5}
r_z	9.84 x10^{-4}
$\dot{r}_x$	1.33 x10^{-5}
$\dot{r}_y$	9.84 x10^{-4}
$\dot{r}_z$	1.33 x10^{-5}

Table III-4 Propagation Results for Circular Formation

State Variable	***% Difference Between Initial and Final Values***
r_x	9.32 x10^{-4}
r_y	3.15 x10^{-4}
r_z	9.32 x10^{-4}
$\dot{r}_x$	3.15 x10^{-4}
$\dot{r}_y$	9.32 x10^{-4}
$\dot{r}_z$	3.15 x10^{-4}

Table III-5 Propagation Results for Projected Circular Formation

State Variable	***% Difference Between Initial and Final Values***
r_x	9.30 x10^{-4}
r_y	3.13 x10^{-4}
r_z	9.30 x10^{-4}
$\dot{r}_x$	3.16 x10^{-4}
$\dot{r}_y$	9.30 x10^{-4}
$\dot{r}_z$	3.16 x10^{-4}

IV. ELLIPTIC REFERENCE ORBIT

A. PROBLEM DEFINITION

In many applications, it is desirable to design formations with non-circular reference orbits. The equations of motion from Chapter III are inapplicable for elliptical reference orbits.[17, 27] This chapter addresses these formations; in particular, the design of new formations using the method described in Chapter II.

Using the same coordinate system as the previous chapter, an additional state was added to simplify the equations of motion. Adding ν, or True Anomaly, the state vector becomes

$$\mathbf{x} = \begin{bmatrix} r_x & r_y & r_z & \dot{r}_x & \dot{r}_y & \dot{r}_z & m & \nu \end{bmatrix}^{\mathrm{T}} \tag{4.1}$$

The controls, representing both a positive and negative thrust direction for each axis, are

$$\mathbf{u} = \begin{bmatrix} T_{x+} & T_{x-} & T_{y+} & T_{y-} & T_{z+} & T_{z-} \end{bmatrix}^{T} \tag{4.2}$$

and were constrained by,

$$0 \le T_{x+}, T_{x-}, T_{y+}, T_{y-}, T_{z+}, T_{z-} \le T_{max} \tag{4.3}$$

The rationale for choosing the controls above was mainly for mathematical and numerical purposes. In calculating both the mass flow and cost of the solution, it is necessary to calculate a total thrust value. Normally this is done by taking the sum of the absolute value for the individual thrust variable which presents mathematical challenges due to non-differentiability. That is, the absolute value of any variable is defined as

$$|x| \triangleq \begin{cases} x & x \ge 0 \\ -x & x < 0 \end{cases} \tag{4.4}$$

It is evident that at $x = 0$, the absolute value function becomes nondifferentiable. This can be avoided by using

$$|x| = \sqrt{x^2} \tag{4.5}$$

but even this introduces numerical issues since the derivative of the square root function is undefined at $x = 0$, which is of great concern since $T_i = 0$ is not only possible, but desired.

One workable solution is to use a different thrust variable for the positive and negative directions. This choice models real life more closely since actual thrusters are capable of firing only in one direction. More importantly, it removes the numerical difficulties by allowing total thrust to be defined as

$$T = \sum \mathbf{u}^i = T_{x+} + T_{x-} + T_{y+} + T_{y-} + T_{z+} + T_{z-} \tag{4.6}$$

This implementation does produce an additional concern since $T_i = 0$ is no longer internal to the constraints on the controls therefore making the constraints active. Activation of the Lagrange multiplier for the controls does not change the problem, but it does make the analysis and validation a bit more involved. **Note that T does not represent the magnitude of the thrust vector**. It has been redefined according to equation (4.6).

For this formation, the path constraint is defined by,

$$d_l^2 \le \left(r_x^2(\tau) + r_y^2(\tau) + r_z^2(\tau) \right) \le d_u^2 \qquad \forall \tau \tag{4.7}$$

where, d_l and d_u are minimum and maximum distance from the reference point to any spacecraft in the swarm. The cost function is

$$J = \frac{1}{\tau_f - \tau_0} \int_{\tau_0}^{\tau_f} T \, d\tau \tag{4.8}$$

It is obvious that if the optimal cost turns out to be zero, then the solution corresponds to a zero-propellant formation; otherwise, the optimal (i.e. minimum fuel) open-loop controls to achieve the desired formation are obtained.

B. EQUATIONS OF MOTION

Since dynamics from Chapter III are invalid for an elliptical reference orbit, a new set of equations must be used. These equations of motion are described in References 17

and 27 and are derived here for the purpose of completeness. Following Kane's notation,[28] the superscript N is used to denote the Newtonian or Inertial reference frame. Starting with the most general equation describing the motion of the *unperturbed* reference orbit,

$$\ddot{\mathbf{R}}_{ref}^{N} = -\mu \frac{\mathbf{R}}{|\mathbf{R}|^3} \tag{4.9}$$

The motion of a swarm satellite is given by

$$\ddot{\mathbf{R}}_{sat}^{N} = \ddot{\mathbf{R}}_{ref}^{N} + \ddot{\mathbf{r}}^{N} = -\mu \frac{\mathbf{R}+\mathbf{r}}{|\mathbf{R}+\mathbf{r}|^3} + \mathbf{a}_p^N + \mathbf{a}_T^N \tag{4.10}$$

where

$$|\mathbf{R}+\mathbf{r}|^3 = \left(|\mathbf{R}|^3 + 2(\mathbf{R}\bullet\mathbf{r})|\mathbf{R}| + |\mathbf{r}|^2 |\mathbf{R}|\right)^{3/2} \tag{4.11}$$

If the assumption $|\mathbf{R}| \gg |\mathbf{r}|$ is now introduced,

$$\frac{\mathbf{R}+\mathbf{r}}{|\mathbf{R}+\mathbf{r}|^3} \approx \frac{1}{|\mathbf{R}|^3}\left(\mathbf{R}+\mathbf{r} - 3\frac{\mathbf{R}\bullet\mathbf{r}}{|\mathbf{R}|^2}\mathbf{R}\right) \tag{4.12}$$

The relative dynamics, though still in the inertial frame, can now be described by

$$\ddot{\mathbf{r}}^{N} = \ddot{\mathbf{R}}_{sat}^{N} - \ddot{\mathbf{R}}_{ref}^{N} = \frac{\mu}{|\mathbf{R}|^3}\left(\mathbf{r}^N - 3\frac{\mathbf{R}\bullet\mathbf{r}}{|\mathbf{R}|^2}\mathbf{R}\right) + \mathbf{a}_p^N + \mathbf{a}_T^N \tag{4.13}$$

In order to retrieve the relative dynamics in the formation reference frame, the Transport Theorem for moving coordinate systems must be applied. The formation reference frame is denoted by the superscript B. Generally it is

$$\ddot{\mathbf{r}}^{N} = \ddot{\mathbf{r}}^{B} + \left({}^{N}\dot{\boldsymbol{\omega}}^{B} \times \mathbf{r}\right) + \left({}^{N}\boldsymbol{\omega}^{B} \times {}^{N}\boldsymbol{\omega}^{B} \times \mathbf{r}\right) + 2\left({}^{N}\boldsymbol{\omega}^{B} \times \dot{\mathbf{r}}^{B}\right) \tag{4.14}$$

Solving for $\ddot{\mathbf{r}}^{B}$ yields

$$\ddot{\mathbf{r}}^{B} = \ddot{\mathbf{r}}^{N} - \left({}^{N}\dot{\boldsymbol{\omega}}^{B} \times \mathbf{r}\right) - \left({}^{N}\boldsymbol{\omega}^{B} \times {}^{N}\boldsymbol{\omega}^{B} \times \mathbf{r}\right) - 2\left({}^{N}\boldsymbol{\omega}^{B} \times \dot{\mathbf{r}}^{B}\right) \tag{4.15}$$

For an unperturbed orbit around a central body, using the perifocal inertial coordinate system,

$$ {}^{N}\boldsymbol{\omega}^{B} = \begin{bmatrix} 0 & 0 & \dot{\nu} \end{bmatrix}^{\mathrm{T}} \qquad and \qquad {}^{N}\dot{\boldsymbol{\omega}}^{B} = \begin{bmatrix} 0 & 0 & \ddot{\nu} \end{bmatrix}^{\mathrm{T}} \tag{4.16} $$

The above equations imply that there cannot be a satellite at the reference point, since it is defined as an unperturbed reference orbit. The definition of angular momentum for any unperturbed orbit,[29]

$$ h = R^2\dot{\nu} = \sqrt{\mu a\left(1-e^2\right)} = na^2\sqrt{1-e^2} \tag{4.17} $$

solving for $\dot{\nu}$,

$$ \dot{\nu} = \frac{na^2}{R^2}\sqrt{1-e^2} \qquad with \qquad a = \frac{R\left(1+e\cos\left(\nu\right)\right)}{\left(1-e^2\right)} \tag{4.18} $$

finally yielding

$$ \dot{\nu} = \frac{n\left(1-e\cos\left(\nu\right)\right)^2}{\left(1-e^2\right)^{3/2}} \tag{4.19} $$

Differentiating equation (4.19) with respect to time produces

$$ \ddot{\nu} = \frac{-2ne\sin(\nu)\dot{\nu}}{\left(1-e^2\right)^{3/2}}\left(1+e\cos(\nu)\right) \tag{4.20} $$

One additional term, $\mathbf{a}_T$, is defined as follows

$$ \mathbf{a}_T = \frac{1}{m}\begin{bmatrix} T_x \\ T_y \\ T_z \end{bmatrix} = \frac{1}{m}\begin{bmatrix} T_{x+} - T_{x-} \\ T_y - T_{y-} \\ T_z - T_{z-} \end{bmatrix} \tag{4.21} $$

Substituting equations (4.13), and (4.16) through (4.21) into equation (4.15) provides the relative dynamical equations of motion in the relative coordinate frame. They are

$$\ddot{\mathbf{r}}^B = \begin{bmatrix} 0 & 2\dot{\nu} & 0 \\ -2\dot{\nu} & 0 & 0 \\ 0 & 0 & 0 \end{bmatrix} \dot{\mathbf{r}}^B + \begin{bmatrix} \dot{\nu}^2 + 2k & \ddot{\nu} & 0 \\ -\ddot{\nu} & \dot{\nu}^2 - k & 0 \\ 0 & 0 & -k \end{bmatrix} \mathbf{r} + \frac{1}{m} \begin{bmatrix} T_x \\ T_y \\ T_z \end{bmatrix} + \mathbf{a}_p^B \tag{4.22}$$

with

$$k = n^2 \left(\frac{1 + e\cos(\nu)}{1 - e^2} \right)^3 \tag{4.23}$$

and an additional dynamic equation needed for the mass flow,

$$\dot{m} = \frac{-T}{v_e} \tag{4.24}$$

One significant fact is that these equations are non-linear in mass. In order to limit the scope of this chapter, problems were confined to a zero perturbation case by setting $\mathbf{a}_p = 0$. It should be noted, however, that the effects of any modelable perturbing force may be included in $\mathbf{a}_p$ as desired to increase the fidelity of the model.

C. NATURAL SOLUTIONS

The first set of solutions are *Natural* solutions for varying eccentricities of the reference orbit. Natural is meant to denote that they require no thrust to maintain configuration and are at least partially periodic satisfying the traditional formation preconceptions. They are of course, only as good as the dynamical model used to find them.

1. Natural Formation for $e = 0.5$

The solution was found in normalized units, allowing it to be applied for any desired formation distance, RU. For the purpose of clarity and comparison, the solutions will be presented in nondimensional units. Table IV-1 itemizes the constraints in place for this formation.

Figure IV-1 shows the three-dimensional view of the formation relative motion. Figure IV-2 shows the orthogonal projection of the relative orbit in the radial versus along-track plane. Figure IV-3 shows the projection in the cross-track versus radial plane while Figure IV-4 projects the orbit onto the cross-track versus along-track plane. As with the previous figures, the X is the location of the reference point. From these results, position appears to be naturally constrained. In other words, the relative orbit is fully periodic even though the constraints are imposed for partial periodicity in velocity. This can be explained by the fact that a fully periodic solution would satisfy the constraints for a partially periodic solution. Additionally, since velocity was constrained, natural orbital motion will tend to drive position toward the periodic solution. This is not a law, since it is possible to find a formation that is periodic in velocity but not in position. On the other hand, if the position is constrained with velocity free, the formations will return to their original position but the velocity may be so large as to make this return impossible. This is of course, "undesirable" for formation configurations.

Table IV-1 Constraints for Natural Formation with $e = 0.5$

Constraint	***Normalized Lower and Upper Bounds***
States: r_x, r_y, r_z	Unconstrained
States: $\dot{r}_x, \dot{r}_y, \dot{r}_z$	Unconstrained
States: m	[0.1 : 1.0]
Controls: $\mathbf{T}$	[0 : Unconstrained]
Time: τ	[0 : 5]
Events: $\mathbf{r}(\tau_0) - \mathbf{r}(\tau_f)$	Unconstrained
Events: $\dot{\mathbf{r}}(\tau_0) - \dot{\mathbf{r}}(\tau_f)$	[0.0 : 0.0]
Path: $g = r_x^2 + r_y^2 + r_z^2$	[2 : 22]
Number of Nodes	199
Reference Orbit: e	0.5

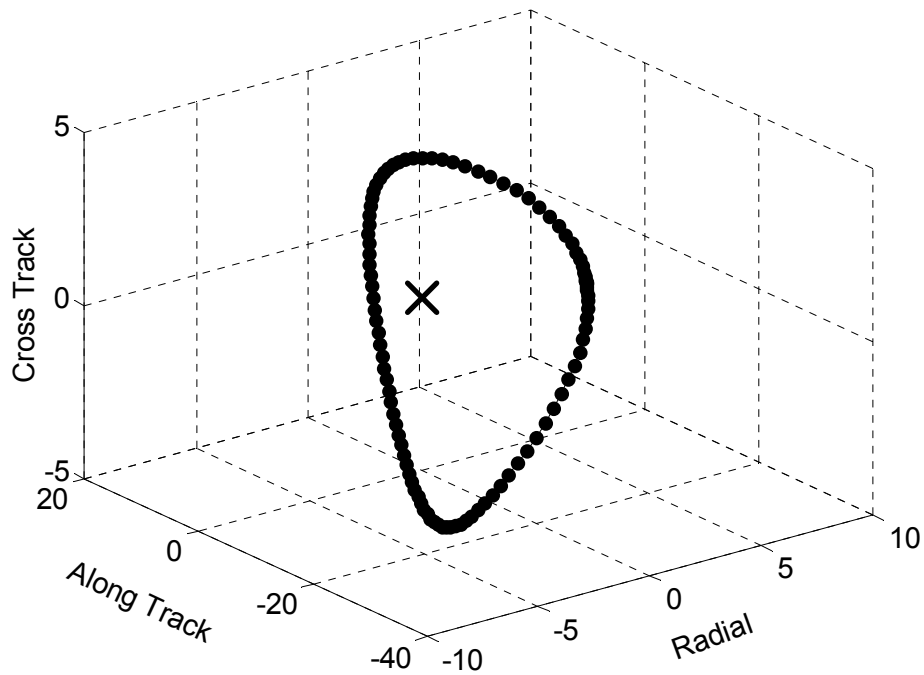

Figure IV-1 3-Dimensional Formation Trajectory for $e = 0.5$ Natural Formation

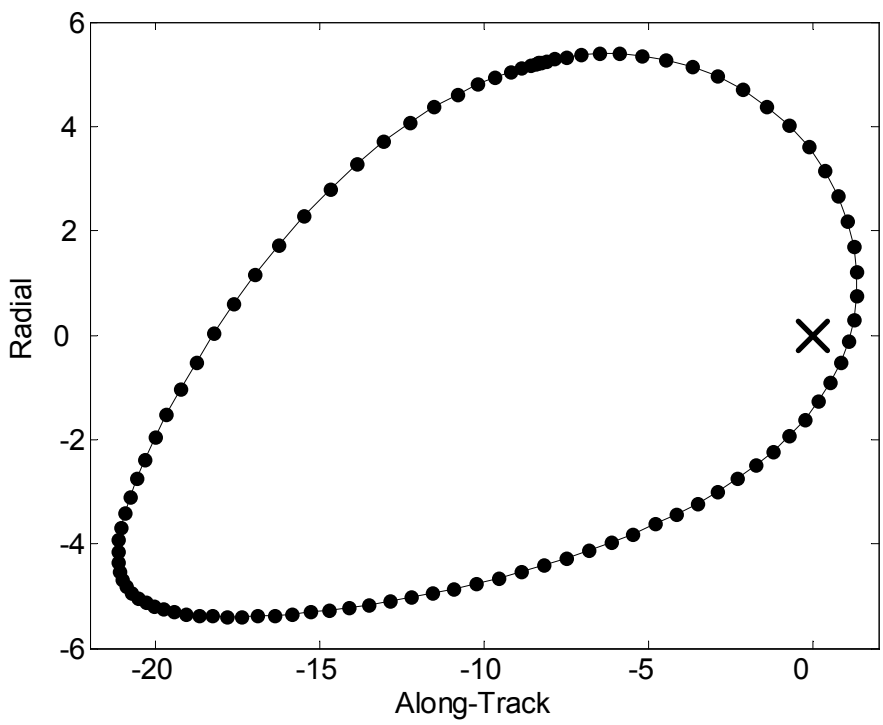

Figure IV-2 Radial vs. Along-Track Motion for $e = 0.5$ Natural Formation

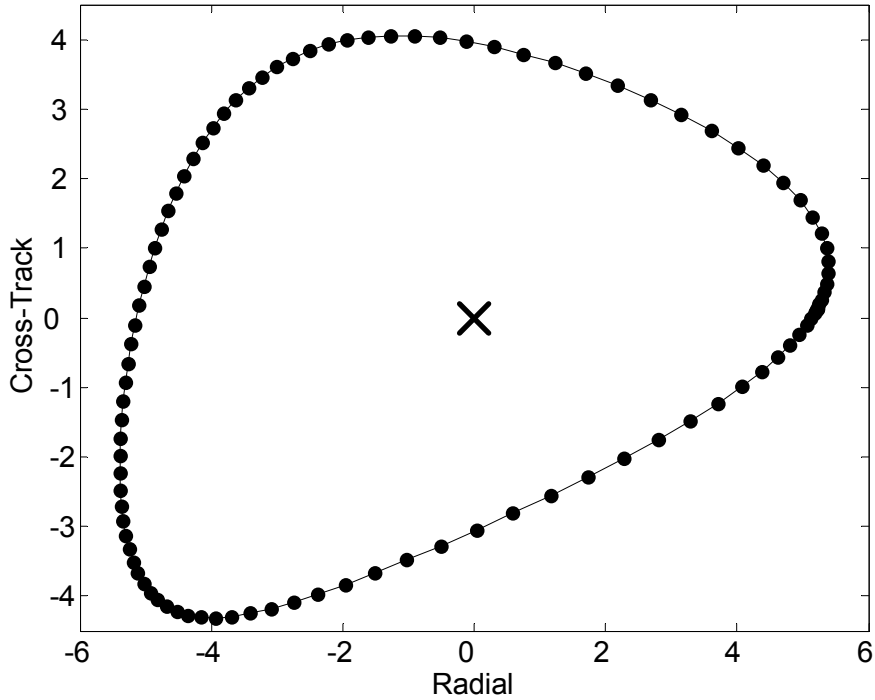

Figure IV-3 Cross-Track vs. Radial Motion for $e = 0.5$ Natural Formation

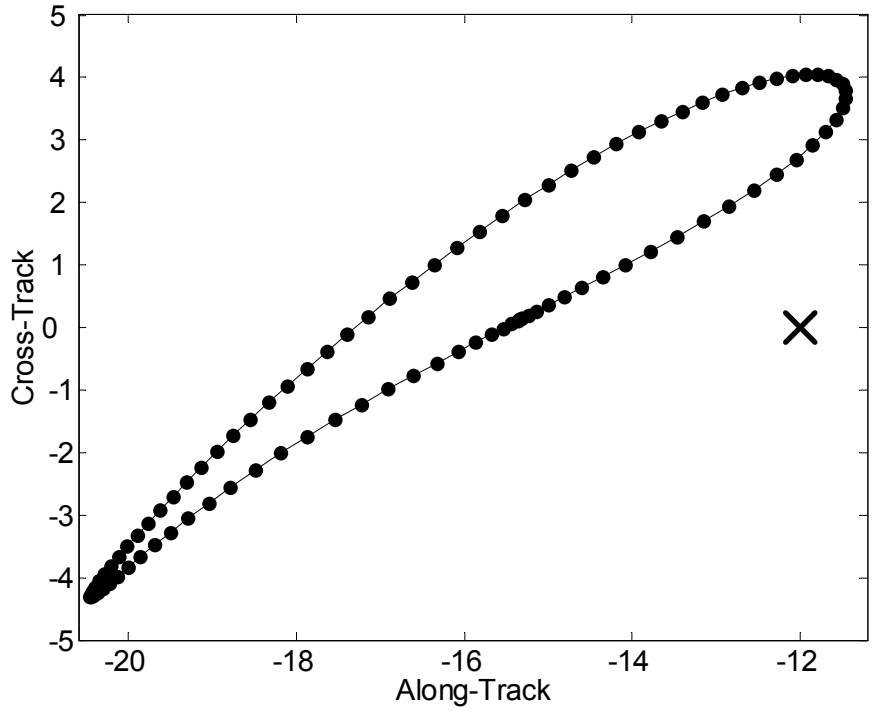

Figure IV-4 Cross-Track vs. Along-Track Motion for $e = 0.5$ Natural Formation

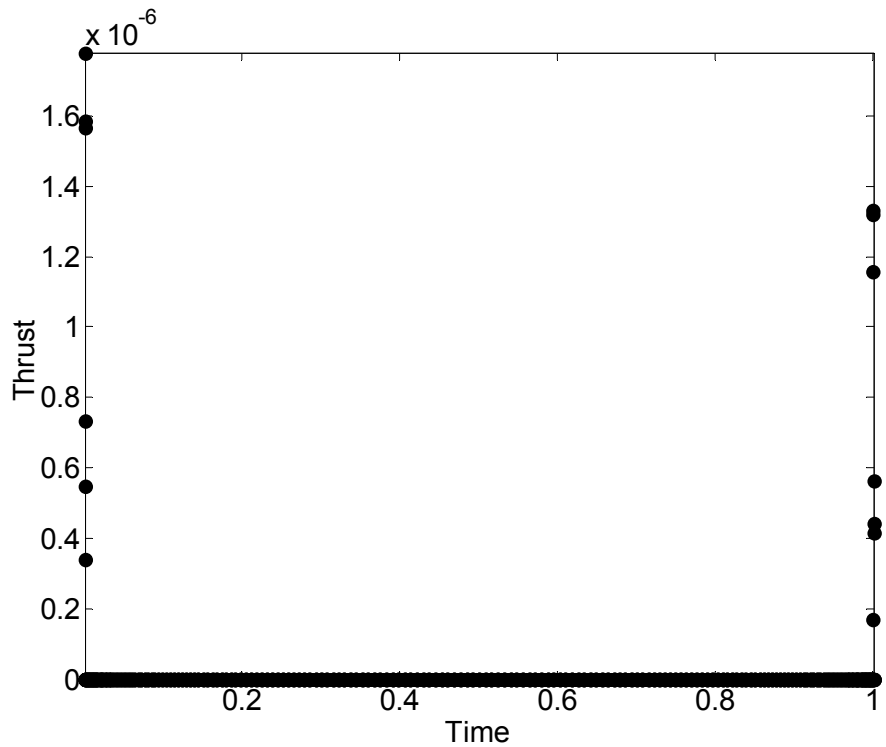

Figure IV-5 Thrust Profile for $e = 0.5$ Natural Formation

Of course, all these results are within numerical tolerances arbitrarily chosen to be 10^{-6} in normalized units. It turns out that the error in the position vector is within 10^{-7} units after one orbit. From Figure IV-5, above, it is clear that this is a zero-propellant formation configuration.

2. Natural Formation for $e = 0.3$

Solution Two is another new formation configuration using the constraints shown in Table IV-2, specifically with $e = 0.3$. Similar to solution one, the time unit, TU, was calculated for a reference orbit with a perigee altitude equal to 1000 km. One of the differences between this formation and the previous, aside from reference orbit eccentricity, is the periodicity constraints. This solution was constrained to be periodic in position with velocity free. The previous solution, in section 1, was periodic in velocity with position free. Figure IV-6 shows the three-dimensional trajectory for this orbit in the formation reference frame. Figure IV-7 to Figure IV-9 show the orthogonal projections of the relative orbit. Again, the X in the figures is the location of the

reference point. Finally, Figure IV-10 demonstrates that this is another zero-propellant formation.

Table IV-2 Constraints for Natural Formation with $e = 0.3$

Constraint	***Normalized Lower and Upper Bounds***
States: r_x, r_y, r_z	Unconstrained
States: $\dot{r}_x, \dot{r}_y, \dot{r}_z$	Unconstrained
States: m	[0.1 : 1.0]
Controls: $\mathbf{T}$	[0 : Unconstrained]
Time: τ	[0 : 5]
Events: $\mathbf{r}(\tau_0) - \mathbf{r}(\tau_f)$	[0.0 : 0.0]
Events: $\dot{\mathbf{r}}(\tau_0) - \dot{\mathbf{r}}(\tau_f)$	Unconstrained
Path: $\mathbf{g}$	Unconstrained
Number of Nodes	80
Reference Orbit: e	0.3

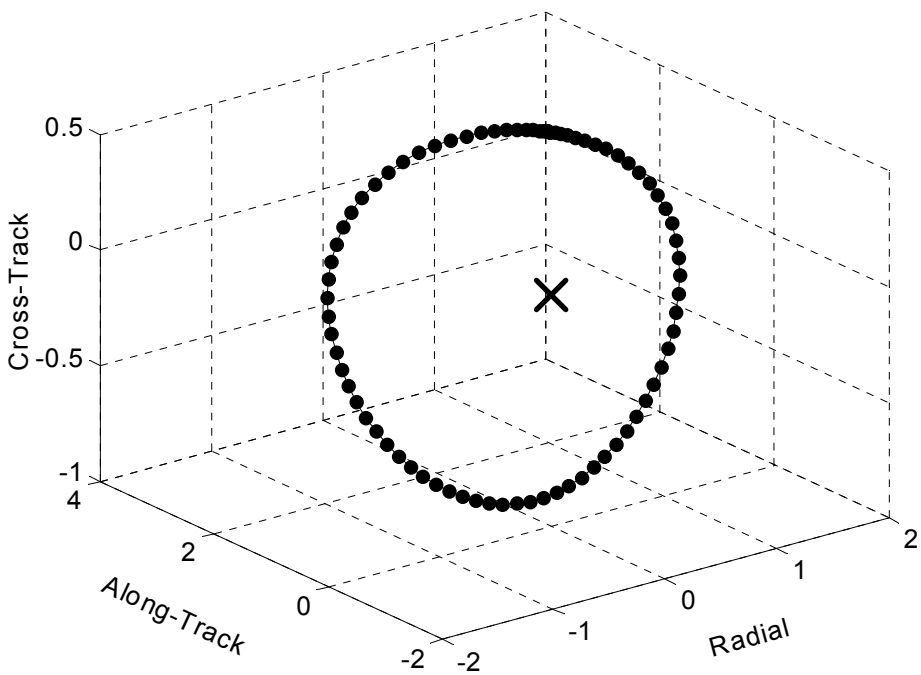

Figure IV-6 3-Dimensional Formation Trajectory for $e = 0.3$ Natural Formation

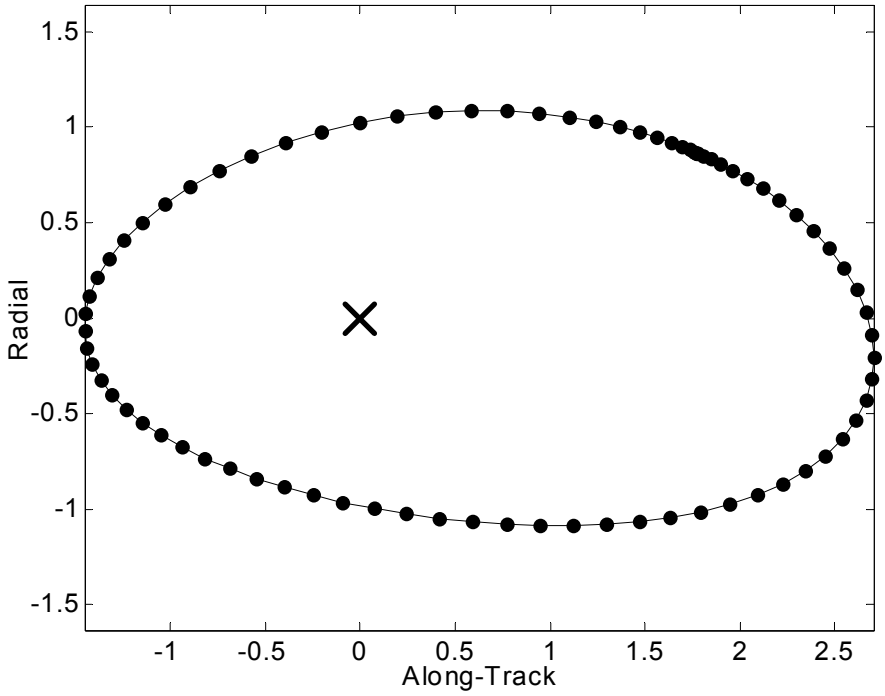

Figure IV-7 Radial vs. Along-Track Motion for $e = 0.3$ Natural Formation

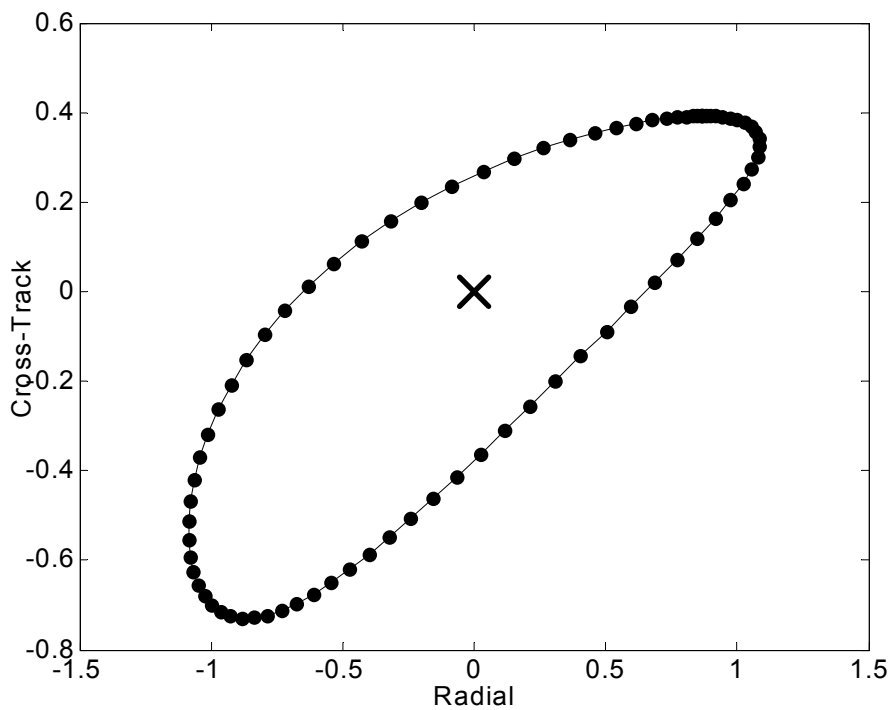

Figure IV-8 Cross-Track vs. Radial Motion for $e = 0.3$ Natural Formation

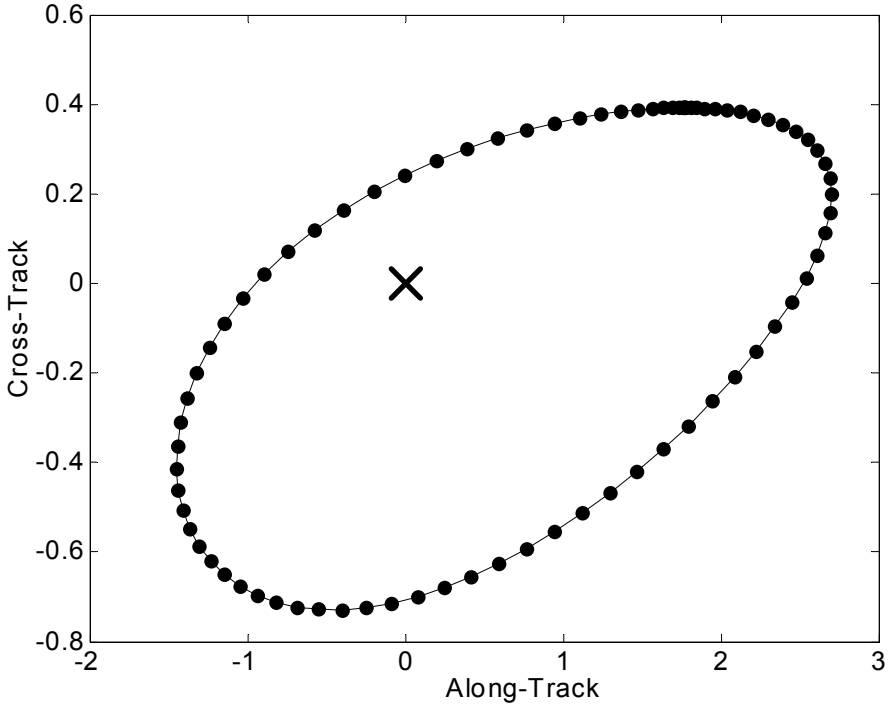

Figure IV-9 Cross-Track vs. Along-Track Motion for $e = 0.3$ Natural Formation

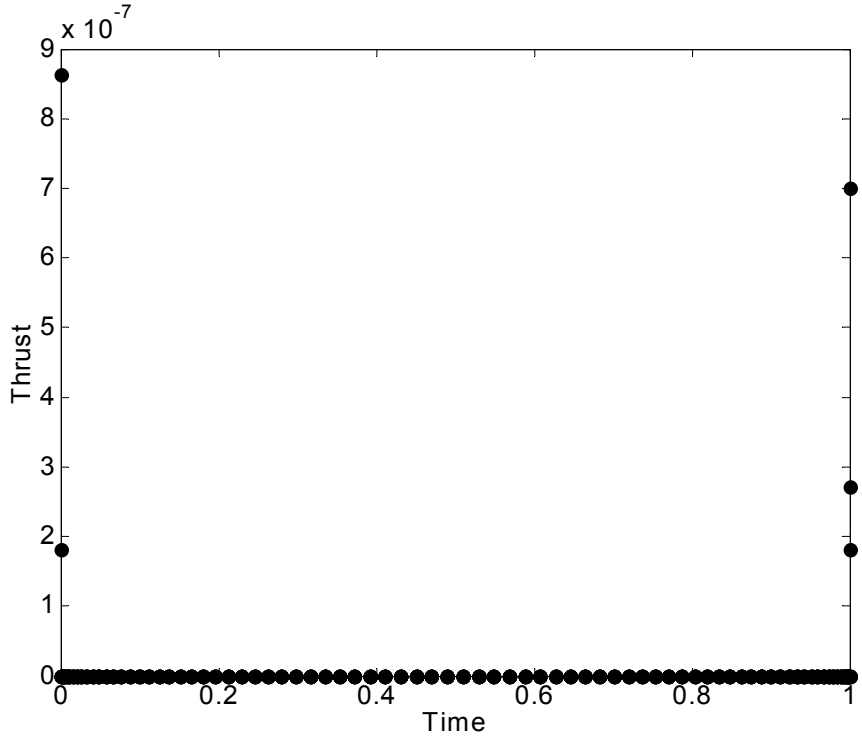

Figure IV-10 Thrust Profile for $e = 0.3$ Natural Formation

3. Natural Formation for $e = 0.7$

Recently, Inhalan et al presented new periodic formations by an analytic method. Solution Three, shown in Figure IV-11 and Figure IV-12, reproduces a particular formation given in Reference 17 for $e = 0.7$ using this method.

By finding the same solution, the method is again validated against independent results. The solution was found by constraining the position states to a three-dimensional box slightly larger than the proposed solution and using the fully periodic event constraints (see Table IV-3).

Table IV-3 Constraints for Natural Formation with $e = 0.7$

Constraint	***Normalized Lower and Upper Bounds***
States: r_x, r_y, r_z	[±0.62, ±1.4, -5.8:1.0]
States: $\dot{r}_x, \dot{r}_y, \dot{r}_z$	Unconstrained
States: m	[0.1 : 1.0]
Controls: $\mathbf{T}$	[0 : Unconstrained]
Time: τ	[0 : 10]
Events: $\mathbf{r}(\tau_0) - \mathbf{r}(\tau_f)$	[0.0 : 0.0]
Events: $\dot{\mathbf{r}}(\tau_0) - \dot{\mathbf{r}}(\tau_f)$	[0.0 : 0.0]
Path: $\mathbf{g}$	Unconstrained
Number of Nodes	99
Reference Orbit: e	0.7

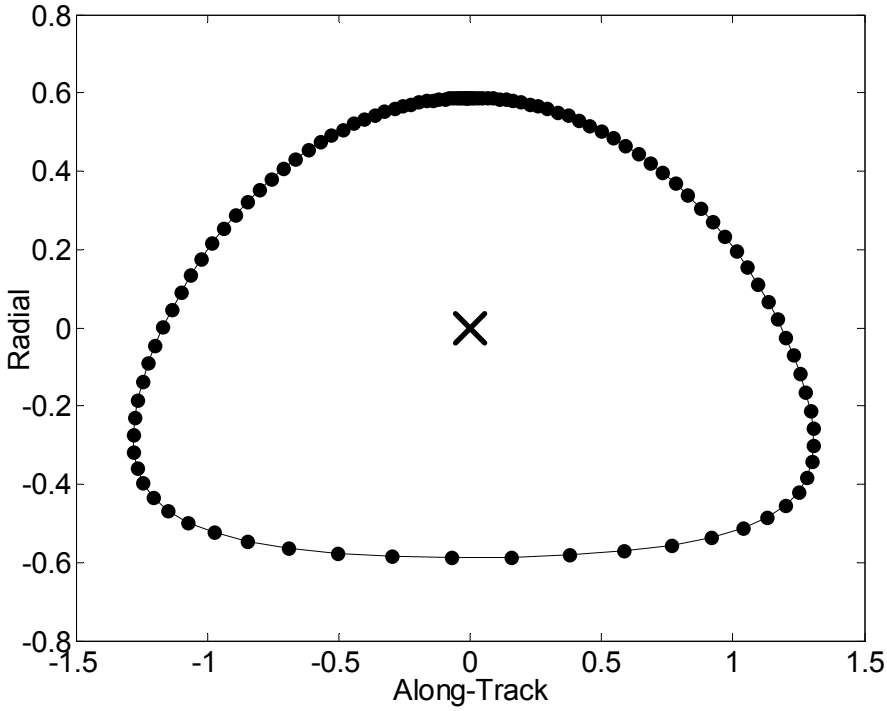

Figure IV-11 Radial vs. Along-Track Motion for $e = 0.7$ Natural Formation

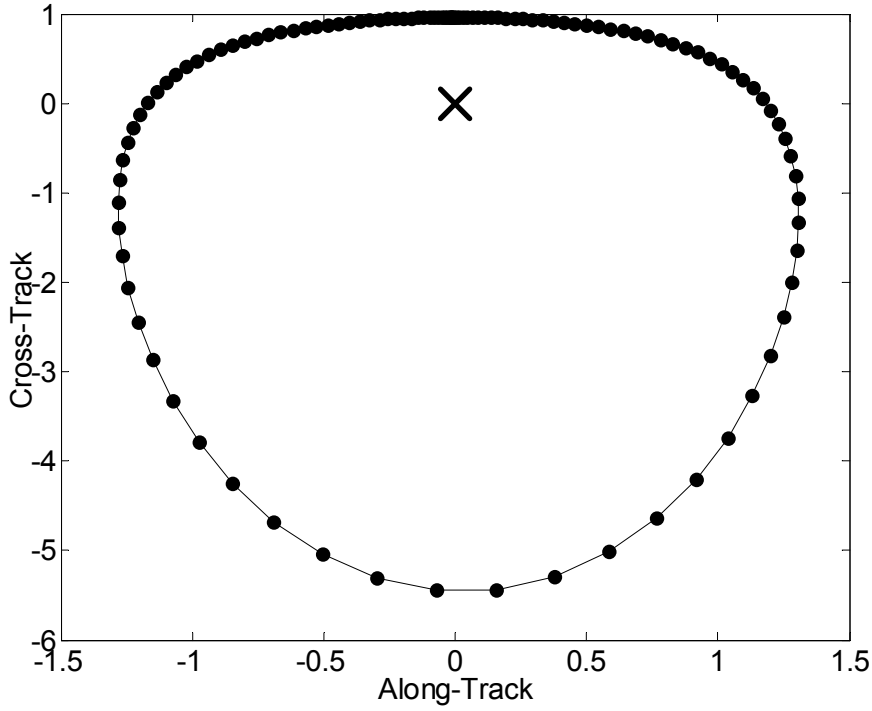

Figure IV-12 Cross-Track vs. Along-Track Motion for $e = 0.7$ Natural Formation

D. FORCED SOLUTIONS

This section provides a glimpse into the power of this method. Specifically, that it can find not only natural formations, but also controlled or ***forced*** formations. These solutions are unique in the sense that Keplerian orbital dynamics cannot produce these formations since they must be actively controlled. This method will determine the feasibility of the formation and will automatically provide the open loop controls required to maintain the desired configuration.

1. Forced Circular Formation

The formation in this section uses a reference orbit eccentricity of 0.3. The configuration constraint is a fixed radius from the reference point. That is, the swarm is restricted to a surface that lies on the sphere $r = constant$. This path constraint is written

$$\mathbf{g} = \left(r_x^2 + r_y^2 + r_z^2\right) = r^2 \tag{4.25}$$

The goal is to minimize the fuel required to meet the configuration constraints shown in Table IV-4. Figure IV-13 shows the three-dimensional plot of the solution formation. It closely resembles Figure III-1, the C-W circular formation, but closer inspection will reveal the subtle differences. Figure IV-14 through Figure IV-16 show the projection of the formation in the three orthogonal planes. Figure IV-17 shows the open loop controls required by one of the satellites to maintain this formation for the given eccentricity. This solution was found using 100 nodes and fixing the final time to exactly one orbit.

Table IV-4 Constraints for Forced Circular Formation

Constraint	***Normalized Lower and Upper Bounds***
States: r_x, r_y, r_z	Unconstrained
States: $\dot{r}_x, \dot{r}_y, \dot{r}_z$	Unconstrained
States: m	[0.1 : 1.0]
Controls: $\mathbf{T}$	[0 : Unconstrained]
Time: τ	$\tau_f = 1.0$
Events: $\mathbf{r}(\tau_0) - \mathbf{r}(\tau_f)$	[0.0 : 0.0]
Events: $\dot{\mathbf{r}}(\tau_0) - \dot{\mathbf{r}}(\tau_f)$	[0.0 : 0.0]
Path: $g = r_x^2 + r_y^2 + r_z^2$	[1.0 : 1.0]
Number of Nodes	100
Reference Orbit: e	0.3

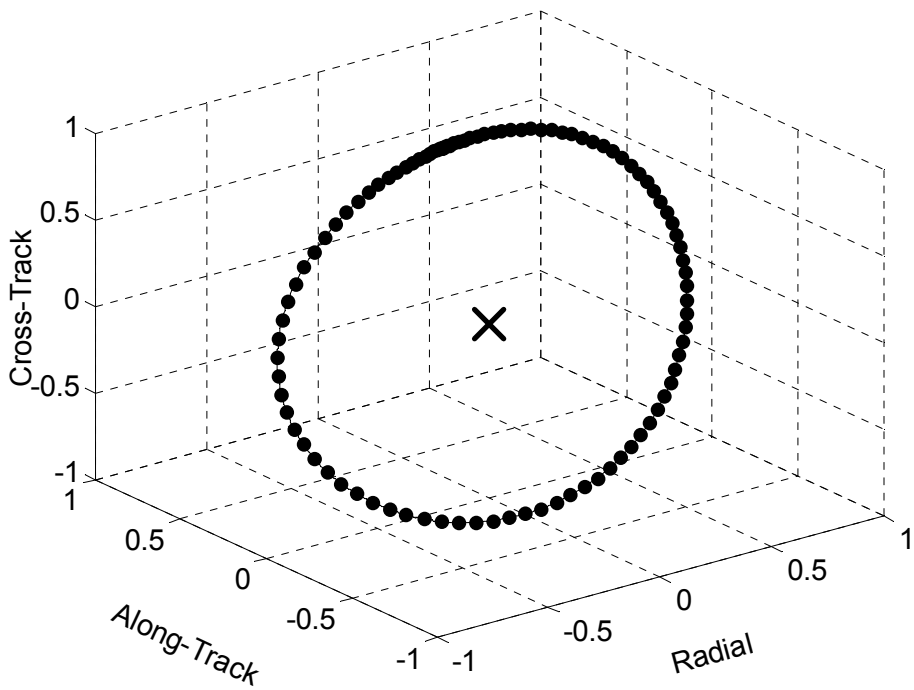

Figure IV-13 Forced Circular Formation for $e = 0.3$

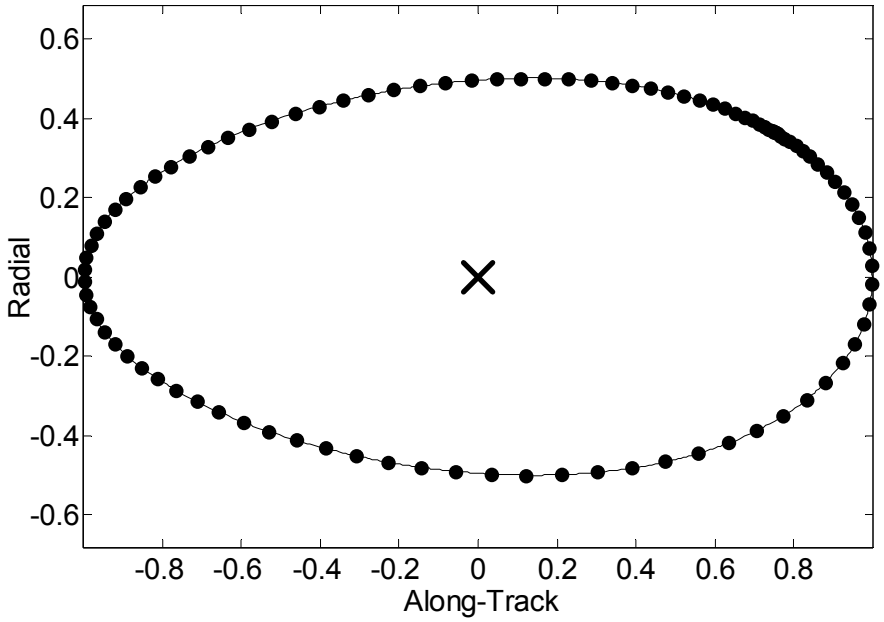

Figure IV-14 Forced Circular Formation Radial vs. Along Track Motion

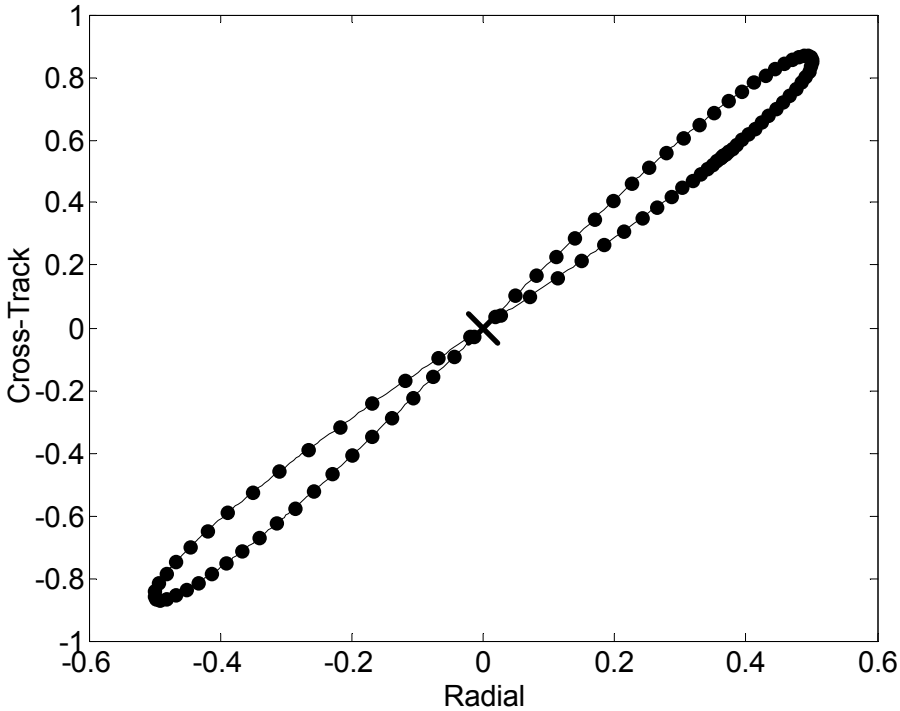

Figure IV-15 Forced Circular Formation Cross-Track vs. Radial Motion

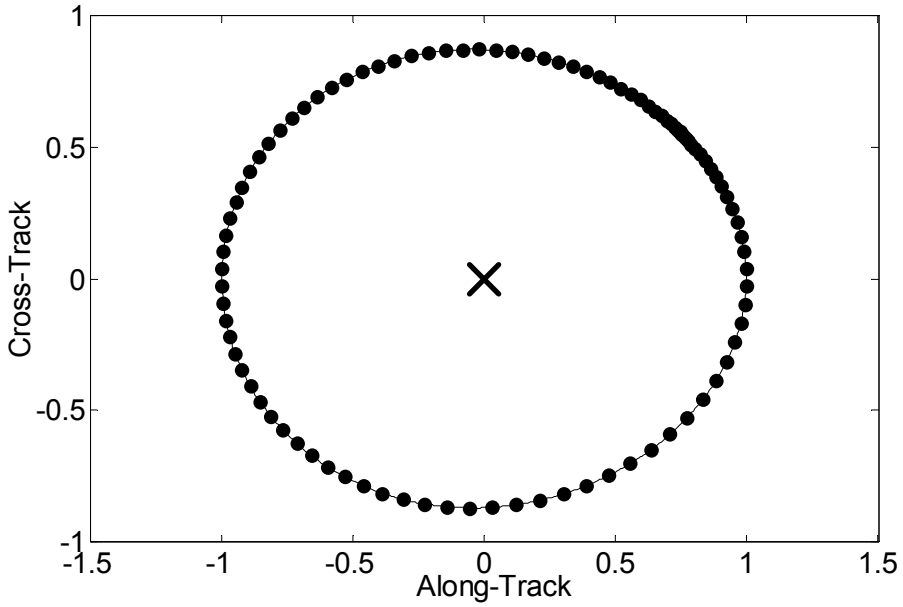

Figure IV-16 Forced Circular Formation Cross-Track vs. Along-Track Motion

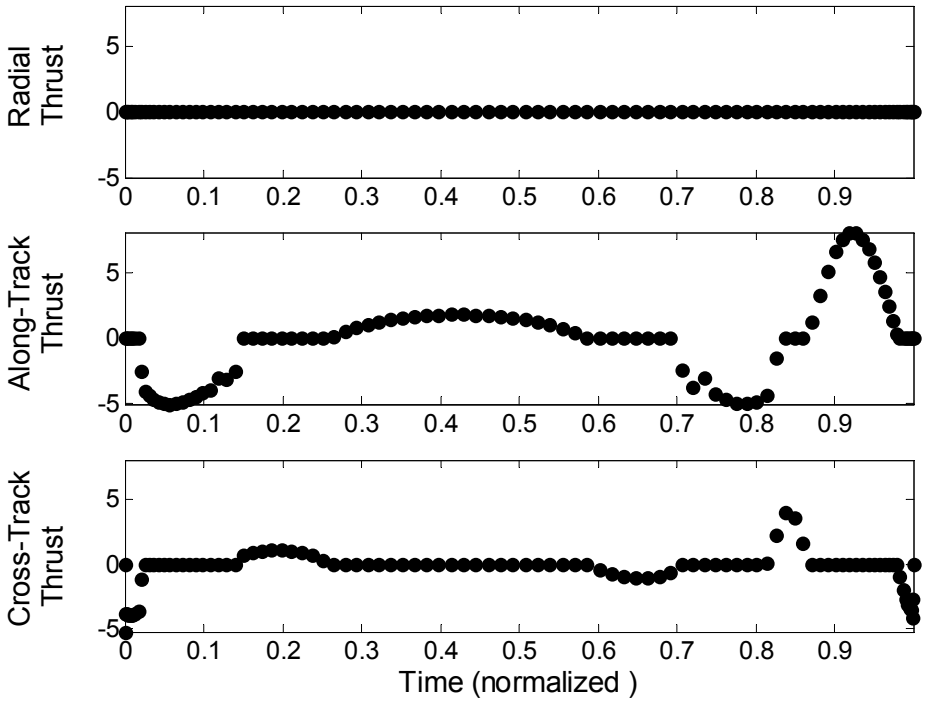

Figure IV-17 Forced Circular Formation Control Thrust Profile

A comparison of Figure IV-15 and Figure III-3 shows the departure from the classic C-W solution. Figure IV-15 apparently shows non-planar motion, but itself is not enough to determine if the formation actually resides in a plane. The answer lies in the angular momentum vector, $\mathbf{h}_{rel} = \mathbf{r} \times \dot{\mathbf{r}}$. The direction of the relative angular moment vector was plotted to determine if the motion was planar. If indeed the motion is planar, then the direction of the angular momentum should remain constant. If the formation is not planar, then the direction of the momentum vector will not be constant. Figure IV-18 shows this plot for the classic C-W circular formation described in section III.D.2 and demonstrates that it is constant, within numeric tolerances. On the other hand, Figure IV-19 shows the same trace for this formation. It is clearly not constant and therefore demonstrates that this formation is non-planar. In both figures, a line is drawn from the origin in the direction of the unit vector associated with the relative angular momentum at the first time step. The dots depict the tip of this angular momentum unit vector at each time step.

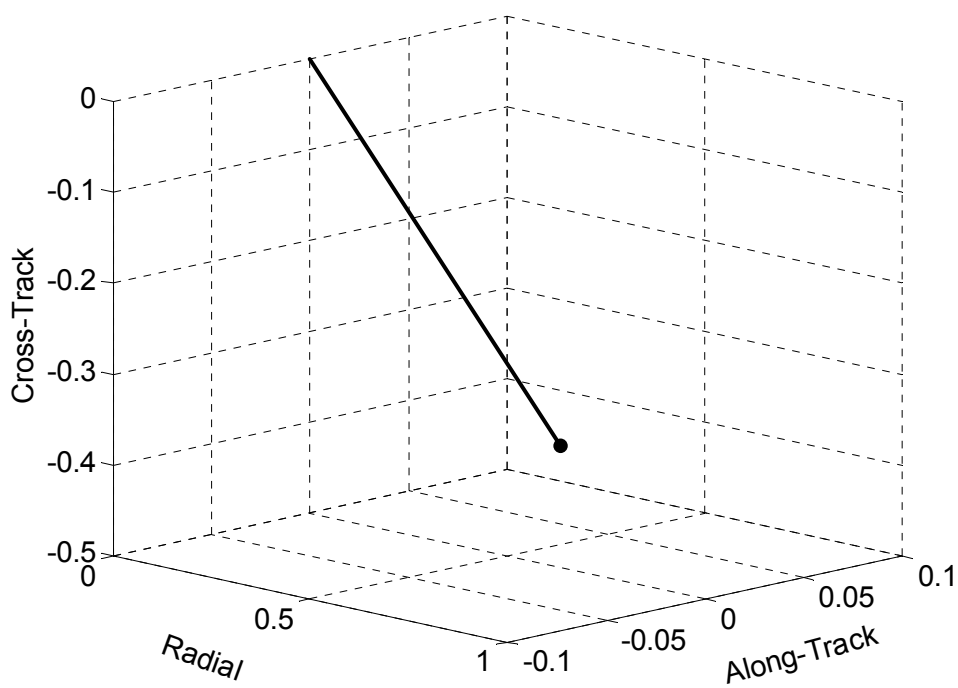

Figure IV-18 Relative Angular Momentum Vector for the C-W Circular Formation

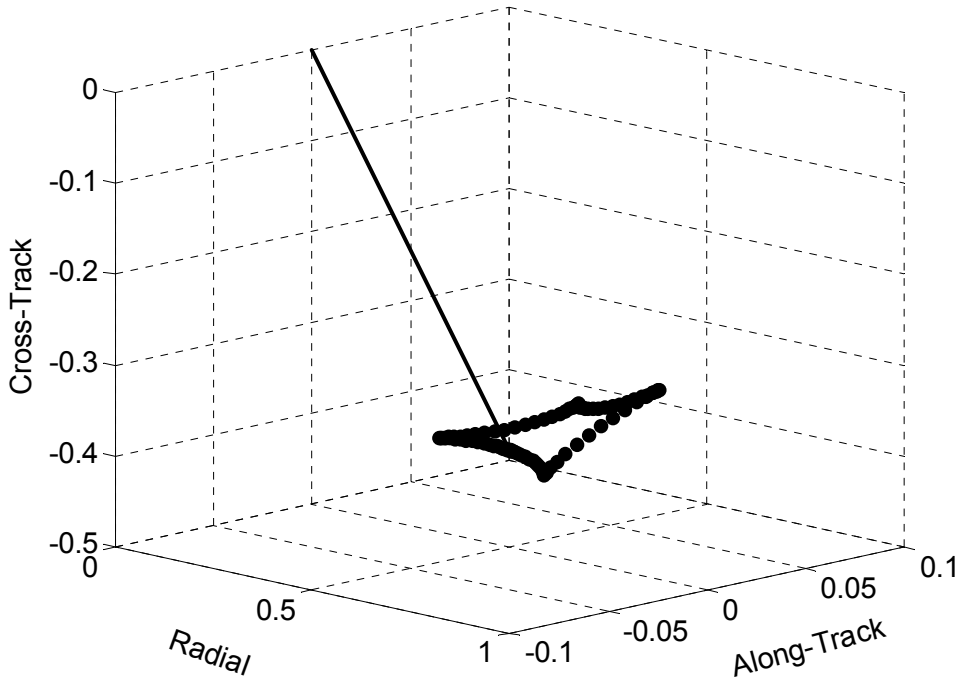

Figure IV-19 Relative Angular Momentum Vector for the Forced Circular Formation

2. Forced Projected Circular Formation

This formation in another example of a forced formation using a well-known configuration. The configuration constraint is the same as seen in section III.D.3, except for a reference orbit eccentricity of 0.3. The goal remains the same: to minimize the fuel required to meet the configuration constraints shown in Table IV-5. Figure IV-20 shows the three-dimensional plot of the solution formation. Figure IV-21 through Figure IV-23 show the projection of this formation in the three orthogonal planes. Figure IV-24 shows the open loop controls required by one of the satellites to maintain this formation for the given eccentricity. This solution was also found using 100 nodes and fixing the final time to exactly one orbit.

Table IV-5 Constraints for Forced Projected Circular Formation

Constraint	***Normalized Lower and Upper Bounds***
States: r_x, r_y, r_z	Unconstrained
States: $\dot{r}_x, \dot{r}_y, \dot{r}_z$	Unconstrained
States: m	[0.1 : 1.0]
Controls: $\mathbf{T}$	[0 : Unconstrained]
Time: τ	$\tau_f = 1.0$
Events: $\mathbf{r}(\tau_0) - \mathbf{r}(\tau_f)$	[0.0 : 0.0]
Events: $\dot{\mathbf{r}}(\tau_0) - \dot{\mathbf{r}}(\tau_f)$	[0.0 : 0.0]
Path: $g = r_y^2 + r_z^2$	[1.0 : 1.0]
Number of Nodes	100
Reference Orbit: e	0.3

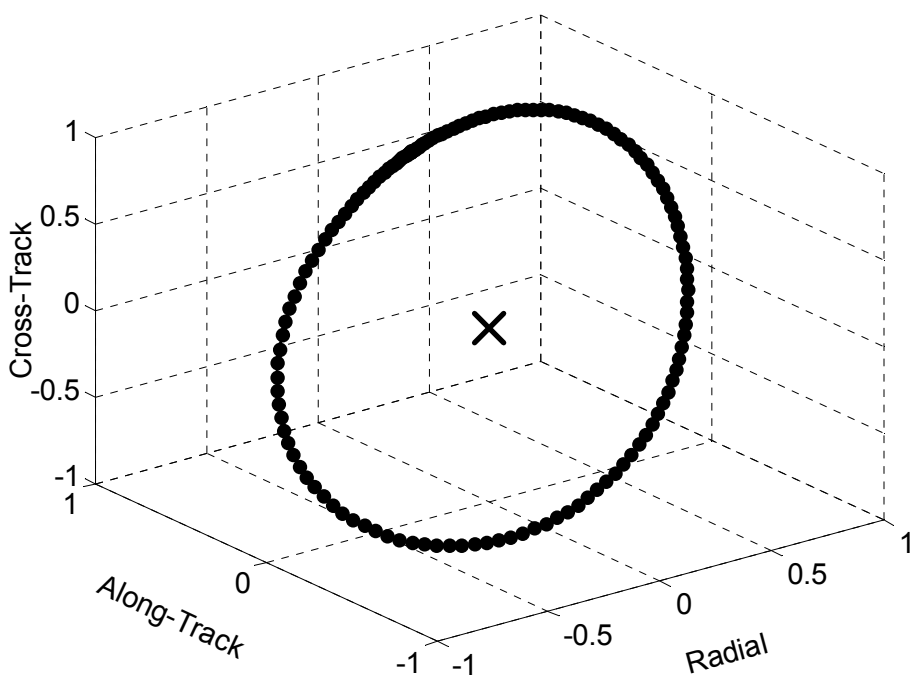

Figure IV-20 Forced Projected Circular Formation for $e = 0.3$

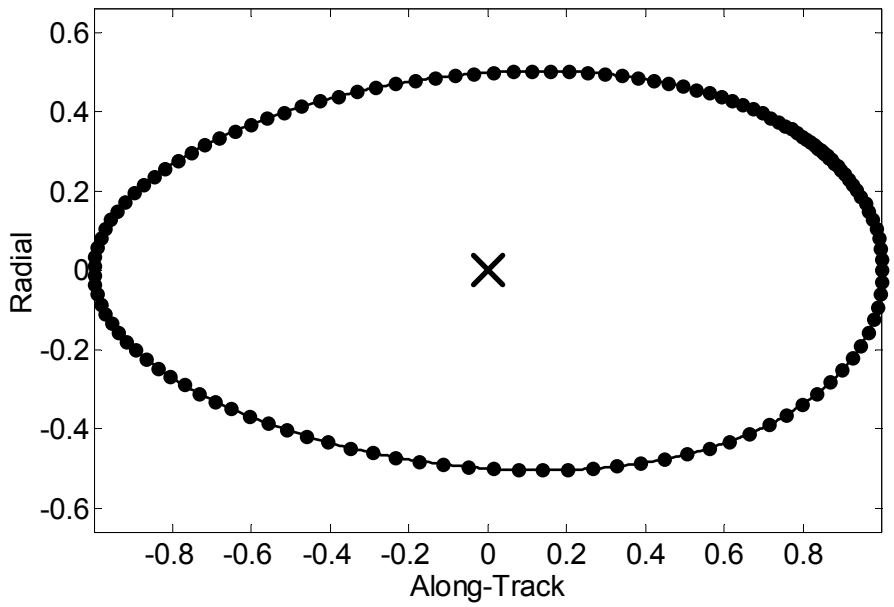

Figure IV-21 Forced Projected Circular Formation Radial vs. Along Track Motion

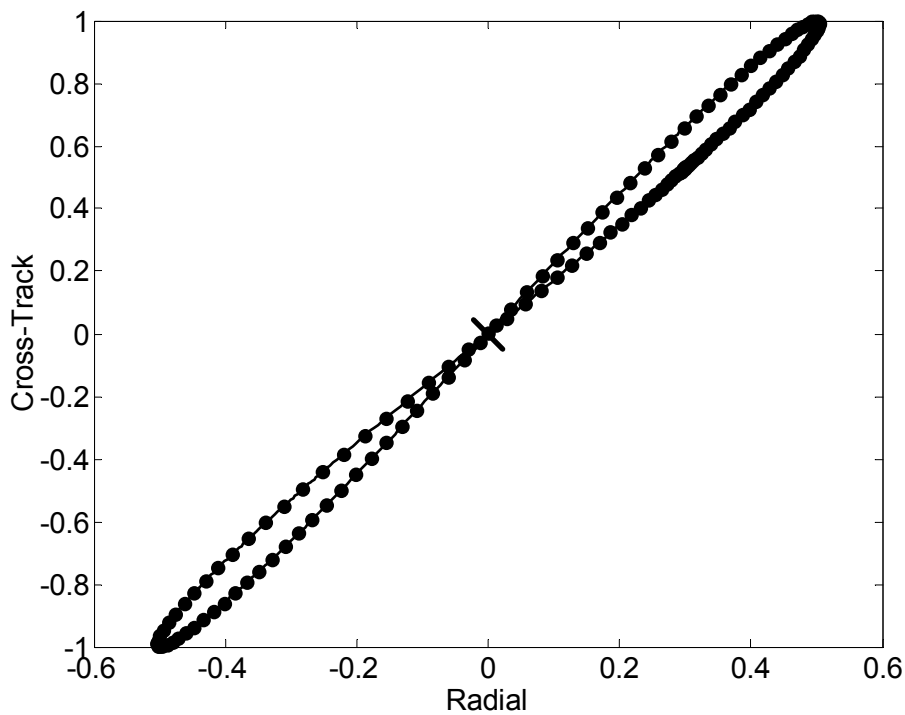

Figure IV-22 Forced Projected Circular Formation Cross-Track vs. Radial Motion

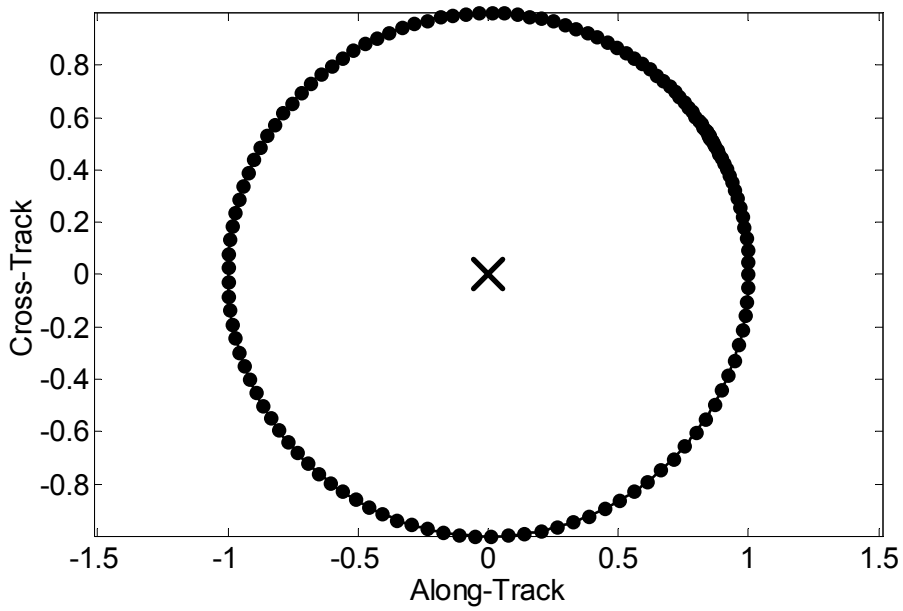

Figure IV-23 Forced Projected Circular Formation Cross-Track vs. Along-Track Motion

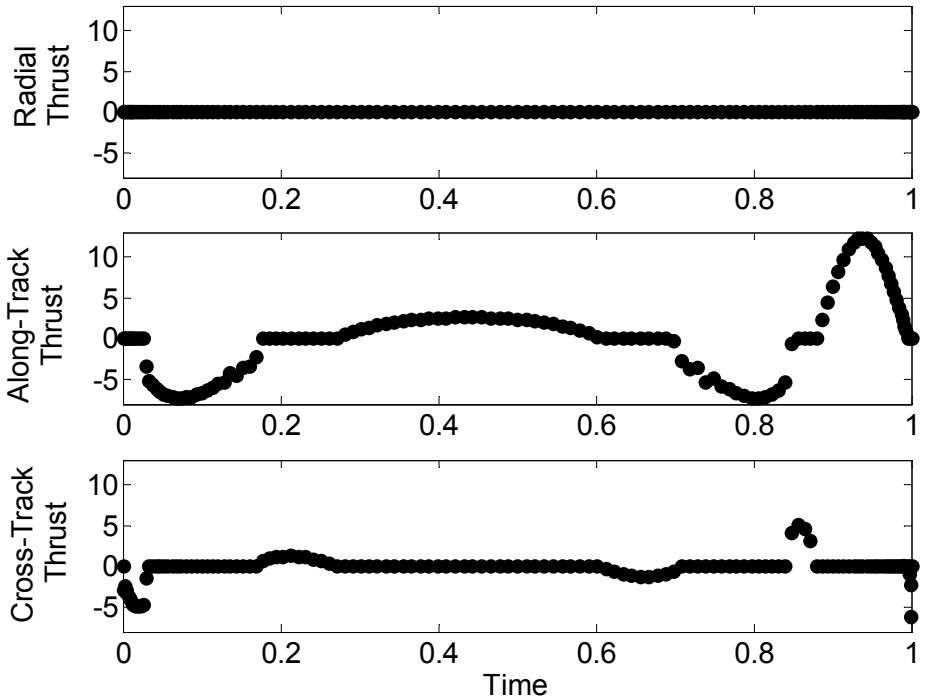

Figure IV-24 Forced Projected Circular Formation Control Thrust Profile

E. VALIDATION OF SOLUTIONS

For all the cases presented here, the following steps were taken in validating the solutions. The Lagrangian was constructed in accordance with section II.B.1 and equation (2.19). Care must be taken to include the state and control bounds in defining the path constraints, $\mathbf{g}$. Taking the partial derivatives of the Lagrangian with respect to the controls yields the following equations:

$$\frac{\partial L}{\partial T_{x+}} = \frac{1}{\tau_f - \tau_0} + \frac{\lambda_{\dot{r}_x}}{m} - \frac{\lambda_m}{v_e} + \phi_{T_{x+}} \tag{4.26}$$

$$\frac{\partial L}{\partial T_{x-}} = \frac{1}{\tau_f - \tau_0} - \frac{\lambda_{\dot{r}_x}}{m} - \frac{\lambda_m}{v_e} + \phi_{T_{x-}} \tag{4.27}$$

$$\frac{\partial L}{\partial T_{y+}} = \frac{1}{\tau_f - \tau_0} + \frac{\lambda_{\dot{r}_y}}{m} - \frac{\lambda_m}{v_e} + \phi_{T_{y+}} \tag{4.28}$$

$$\frac{\partial L}{\partial T_{y-}} = \frac{1}{\tau_f - \tau_0} - \frac{\lambda_{\dot{r}_y}}{m} - \frac{\lambda_m}{v_e} + \phi_{T_{y-}} \tag{4.29}$$

$$\frac{\partial L}{\partial T_{z+}} = \frac{1}{\tau_f - \tau_0} + \frac{\lambda_{\dot{r}_z}}{m} - \frac{\lambda_m}{v_e} + \phi_{T_{z+}} \tag{4.30}$$

$$\frac{\partial L}{\partial T_{z-}} = \frac{1}{\tau_f - \tau_0} - \frac{\lambda_{\dot{r}_z}}{m} - \frac{\lambda_m}{v_e} + \phi_{T_{z-}} \tag{4.31}$$

ϕ is called the switching function for the controls and is governed by the KKT conditions described in equation (2.22). Figure IV-25 shows the switching function for the Thrust in each of the three axes corresponding to the thrust profile shown in Figure IV-24. Not inherently obvious is that the switching function is the same for both circular and projected circular formations at given values of v, since the path constraints are not control dependent.

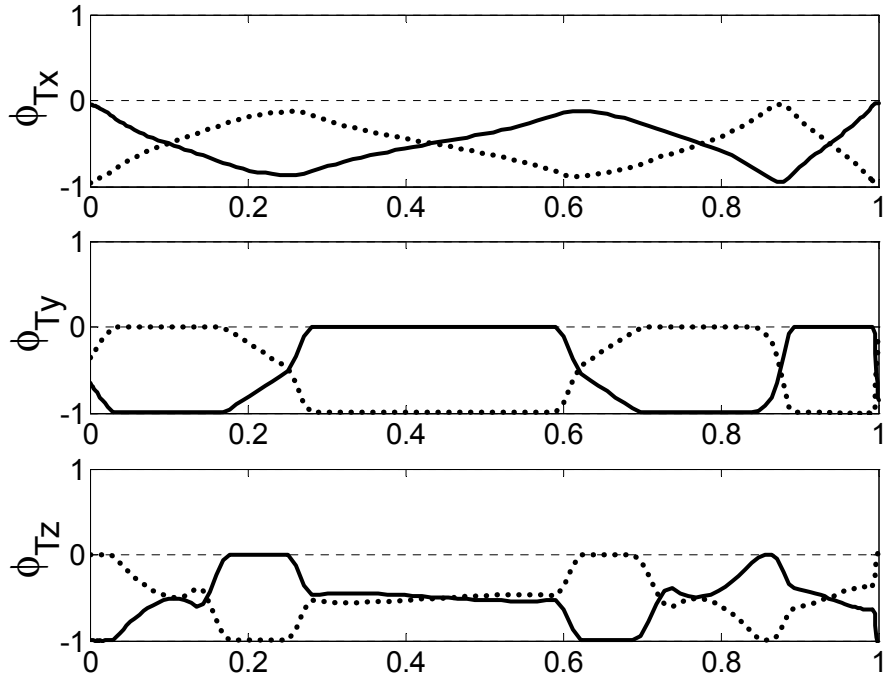

Figure IV-25 Switching Functions for Control Thrust

In addition to the optimality analysis described above, the initial conditions from the DIDO solution were numerically propagated for 50 orbits. For the natural solutions, the initial conditions were propagated with all components of thrust set equal to zero. For the forced solutions, the solution thrust profile was imported into the propagator. This profile was interpolated to determine the value for the controls at each propagation time step. The propagator was free to determine its own time steps, which did not necessarily match the solution time steps. In the process of creating a propagator, every MATLAB resident ODE solver was evaluated. ODE45 proved to have the best combination of accuracy and speed. Additionally, many different interpolation schemes were evaluated. A MATLAB function called POLINT provided the most accurate results. It was created by Weideman and Reddy and implements the barycentric formula from Henrici's *Essentials of Numeric Analysis*. Spline interpolation was the next best in accuracy, and provided a significant benefit in speed over POLINT. Spline was used for routine evaluations and POLINT was reserved for more detailed assessments.

1. Natural Formation for $e = 0.5$

Figure IV-26 and Table IV-6 show that there is no appreciable deviation in formation configuration after being propagated for 50 orbits.

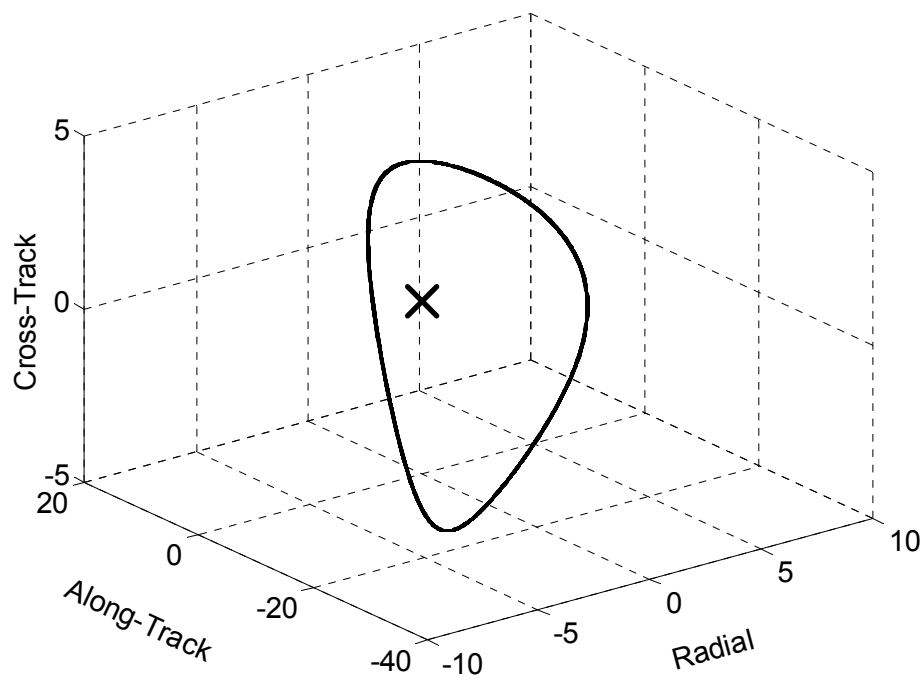

Figure IV-26 Natural Formation with $e = 0.5$ Over 50 Orbits

Table IV-6 Propagation Results for Natural Formation with $e = 0.5$

State Variable	***% Difference Between Initial and Final Values***
r_x	8.54 x10^{-4}
r_y	5.77 x10^{-1}
r_z	4.61 x10^{-5}
$\dot{r}_x$	6.67 x10^{-1}
$\dot{r}_y$	1.04 x10^{-3}
$\dot{r}_z$	2.35 x10^{-4}

2. Natural Formation for $e = 0.3$

Again, the initial conditions were numerically propagated (with thrust equal to zero) for 50 orbits. Figure IV-27 and Table IV-7 show that there is no significant difference over this period.

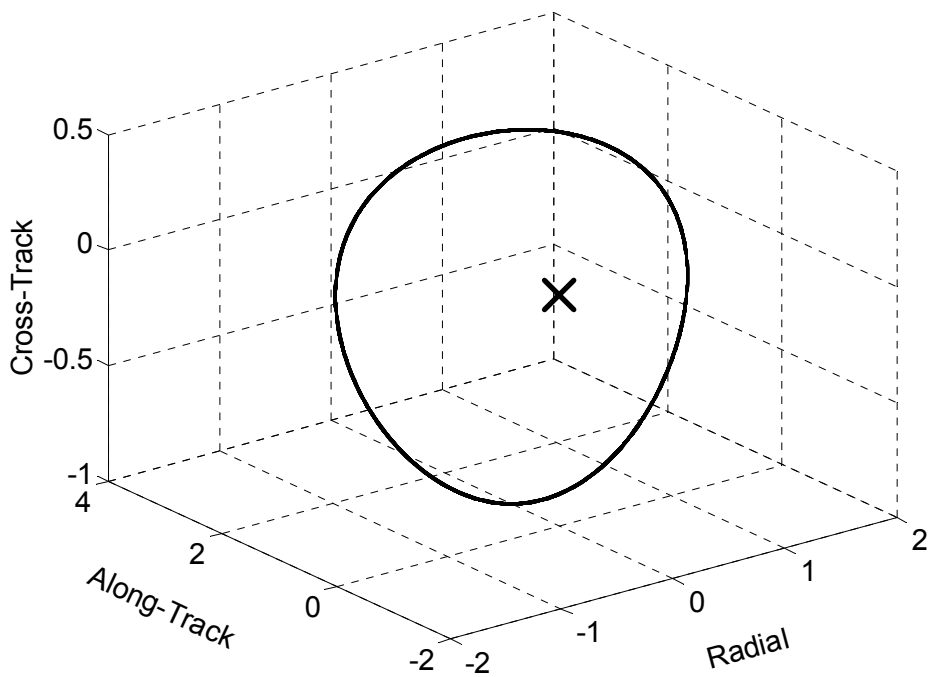

Figure IV-27 Natural Formation with $e = 0.3$ Over 50 Orbits

Table IV-7 Propagation Results for Natural Formation with $e = 0.3$

State Variable	***% Difference Between Initial and Final Values***
r_x	9.06 x10^{-4}
r_y	8.71 x10^{-2}
r_z	1.97 x10^{-4}
$\dot{r}_x$	5.73 x10^{-2}
$\dot{r}_y$	1.11 x10^{-3}
$\dot{r}_z$	6.67 x10^{-5}

3. Natural Formation for $e = 0.7$

Since solution three is a reproduction of a previously known solution, the validation of the formation configuration can be found in Reference 17.

4. Forced Circular Formation

The validation of this result included propagating the initial conditions numerically for 50 orbits, now subject to the thrust profile shown in Figure IV-17. Figure IV-28 shows the three-dimensional motion of the formation over this time period. Table IV-8 also demonstrates that, as desired, there is no appreciable digression in the formation configuration over 50 orbits.

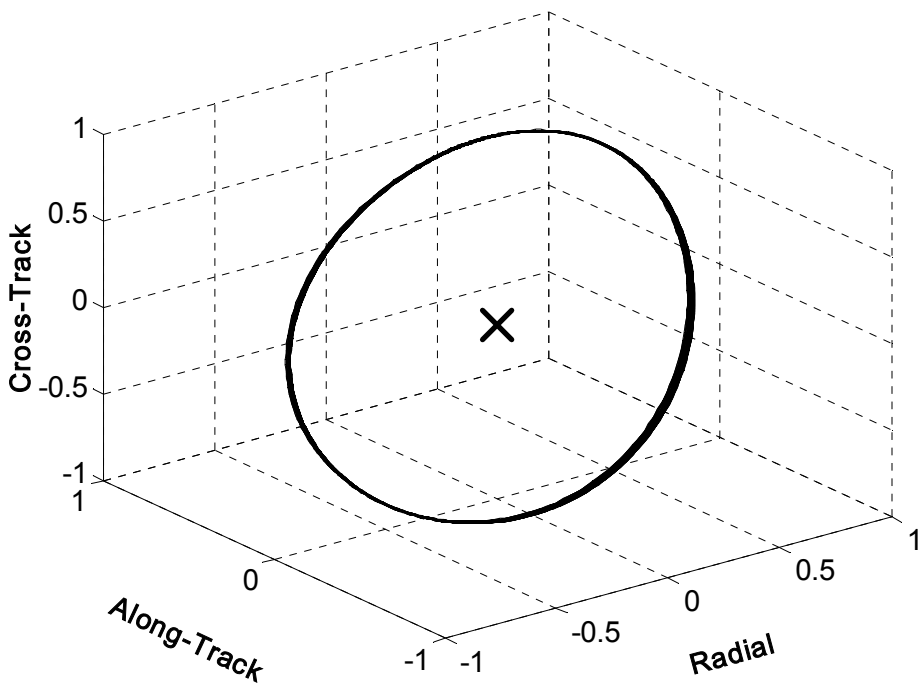

Figure IV-28 Forced Circular Formation over 50 Orbits

Table IV-8 Propagation Results for Forced Circular Formation

State Variable	***% Difference Between Initial and Final Values***
r_x	0.23
r_y	1.51
r_z	0.04
$\dot{r}_x$	0.22
$\dot{r}_y$	0.80
$\dot{r}_z$	0.11

One unique consequence of imposing the circular formation constraint is that it provides another way to verify the results. The forced circular is defined by $r = \text{constant}$ which means $\dot{r} = 0$. This implies $r^2 = \mathbf{r} \cdot \mathbf{r} = \text{const}$, which gives $d/dt\left(r^2\right) = 2\left(\dot{\mathbf{r}} \cdot \mathbf{r}\right) = 0$, followed naturally by

$$\frac{d}{dt}\left(\dot{\mathbf{r}} \cdot \mathbf{r}\right) = \ddot{\mathbf{r}} \cdot \mathbf{r} + \dot{\mathbf{r}} \cdot \dot{\mathbf{r}} = 0 \tag{4.32}$$

Substituting the EOM for $\ddot{\mathbf{r}}$ above provides an independent check that the solution is indeed a circular formation.

5. Forced Projected Circular Formation

As with the previous solutions, the initial conditions were propagated numerically for 50 orbits, subject to the thrust profile shown in Figure IV-24. Figure IV-29 shows the three-dimensional motion of the formation over this time. Table IV-9 also details the errors in the formation configuration after 50 orbits.

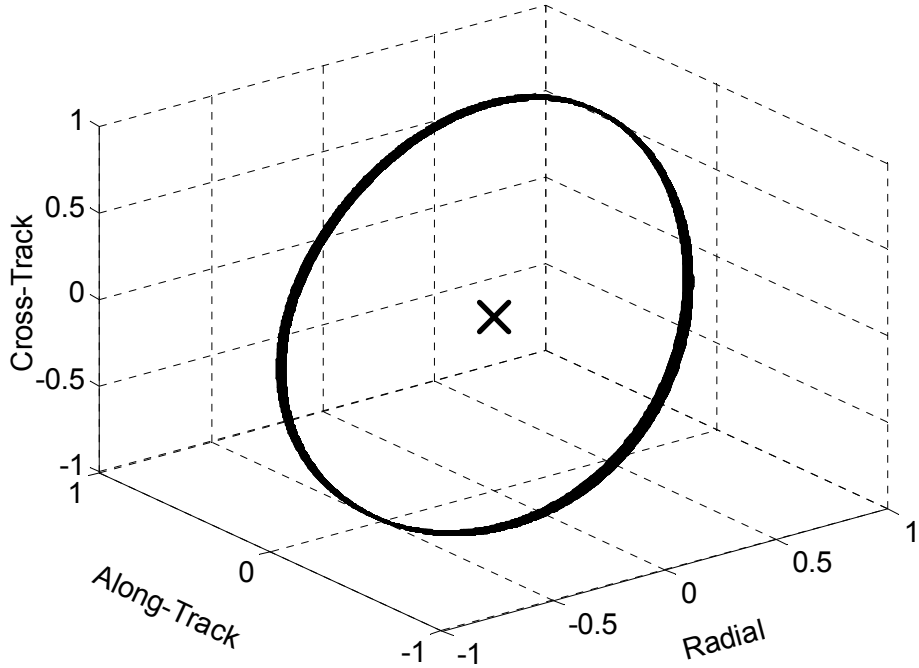

Figure IV-29 Forced Projected Circular Formation over 50 orbits

Table IV-9 Propagation Results for Forced Projected Circular Formation

State Variable	***% Difference Between Initial and Final Values***
r_x	0.06
r_y	1.33
r_z	0.01
$\dot{r}_x$	0.11
$\dot{r}_y$	0.47
$\dot{r}_z$	0.02

THIS PAGE INTENTIONALLY LEFT BLANK

V. UNRESOLVED ISSUES

A. OPTIMAL PERIOD VS. ORBITAL PERIOD

For Natural or Zero-Thrust solutions, the optimal period, $(\tau_f - \tau_0)$, is exactly equal to the orbital period. However, once thrust is required to maintain the formation the optimal period may or may not equal the orbital period. One way to resolve this is to force the solution period to be equal to the orbital period. However, this fix raises several questions.

Table V-1 shows the cost associated with two different solutions to the Forced Circular Formation with $e = 0.3$ and assumes a 100 kg satellite, with $I_{sp} = 1000$ sec, and the TU for a perigee altitude of 1000 km. Solution 1A is detailed in section IV.D.1, while Solution 2A is not shown in the prior chapters. Table V-2 shows the cost associated with two different solutions to the Forced Projected Circular Formation using the same assumptions described above. Solution 1B is represented in section IV.D.2, while Solution 2B is not shown.

Table V-1 Differing Costs for Forced Circular Solutions

Forced Circular Solution 1A	
Cost: $T/(\tau_f - \tau_0)$	1.98 x10^{-7} Newtons/sec
Cost: % Mass	2.34 x10^{-5} %
Optimal Period: τ_f	1.0 orbital periods
Forced Circular Solution 2A	
Cost: $T/(\tau_f - \tau_0)$	1.80 x10^{-7} Newtons/sec
Cost: % Mass	1.00 x10^{-5} %
Optimal Period: τ_f	1.0005 orbital periods

Table V-2 Differing Costs for Forced Projected Circular Solutions

Forced Projected Circular Solution 1B	
Cost: $T/(\tau_f - \tau_0)$	2.87 x10^{-7} Newtons/sec
Cost: % Mass	3.39 x10^{-5} %
Optimal Period: τ_f	1.0 orbital periods
Forced Projected Circular Solution 2B	
Cost: $T/(\tau_f - \tau_0)$	2.85 x10^{-7} Newtons/sec
Cost: % Mass	3.38 x10^{-5} %
Optimal Period: τ_f	1.002 orbital periods

In both cases, the second solution has the lower total cost. However, the optimal period of these solutions is not equal to the orbital period. The precise explanation is unknown. These solutions may be periodic as a formation, but not periodic with respect to the reference point since the period of the reference point (or satellite) is, by definition, equal to the orbital period. This mismatch in periods presents difficulty in visualizing or plotting the configuration or relative motion. If ignored, the formation appears to drift away from the reference point and therefore not stay together. One way to overcome this visualization problem is to display the position of one swarm satellite against another swarm satellite. Over the course of the optimal period, the distance should remain bounded and repeat itself.

B. SWITCHING FUNCTION : DERIVED VS. DIDO SOLUTION

Normally, $\frac{dL}{d\mathbf{T}}$ (see equations (4.26) through (4.31)) is equal to zero for an optimal solution. This allows the values for the switching function, ϕ, to be derived and calculated. At the same time, DIDO calculates the values for the switching function directly. Figure IV-25 shows the switching function as calculated by DIDO, which agrees with the expected results. The concern is that the value for $\frac{dL}{d\mathbf{T}}$ is not 0.0 but

exactly 0.5. The resulting switching functions have the identical shape as those in Figure IV-25, but are offset by negative 0.5 in the vertical axis. This discrepancy in the switching function requires further analysis.

C. J2 PERTURBATIONS

Work was started on implementing the effects of earth oblateness or J_2 in the relative frame, but due to time constraints was not completed.

1. Linear J_2 terms.

The following Linear equations for J_2 effects in the relative frame came from an unpublished paper by I.M. Ross.[30] Using the same coordinate system as Figure II-1 and assuming a circular reference orbit, the J2 effects can be represented as relative accelerations.

$$\mathbf{a}_{J_2} = n^2 J_R \begin{bmatrix} 12\sin^2 i \sin^2 \varpi & -4\sin^2 i \sin 2\varpi & -4\sin 2i \sin \varpi \\ -4\sin^2 i \sin 2\varpi & 1+\sin^2 i\left(2-7\sin^2 \varpi\right) & \sin 2i \cos \varpi \\ -4\sin 2i \sin \varpi & \sin 2i \cos \varpi & 3-\sin^2 i\left(2+5\sin^2 \varpi\right) \end{bmatrix} \begin{bmatrix} r_x \\ r_y \\ r_z \end{bmatrix} \tag{5.1}$$

where

$$J_R = \frac{3J_2 R_e^2}{2R_{ref}^2} \quad \text{and} \quad \varpi = \omega + \nu \tag{5.2}$$

2. Non-linear J_2 terms.

By comparison, the non-linear J_2 terms[20] in the inertial reference frame are

$$a_{\hat{I}_{J_2}} = \frac{J_{R_i} R_{\hat{I}}}{R_{sat}^5}\left(1-\frac{5R_{\hat{K}}^2}{R_{sat}^2}\right) \tag{5.3}$$

$$a_{\hat{J}_{J_2}} = \frac{J_{R_i} R_{\hat{J}}}{R_{sat}^5}\left(1-\frac{5R_{\hat{K}}^2}{R_{sat}^2}\right) \tag{5.4}$$

$$a_{\hat{K}_{J_2}} = \frac{J_{R_i} R_{\hat{K}}}{R_{sat}^5}\left(3-\frac{5R_{\hat{K}}^2}{R_{sat}^2}\right) \tag{5.5}$$

where

$$J_{R_i} = \frac{-3J_2\mu R_e^2}{2} \tag{5.6}$$

In order to get the relative accelerations resulting from J_2 into the relative frame, several transformations must be defined. To transform perifocal to Earth-centered inertial (ECI):

$$\left[\frac{IJK}{PQW}\right] = \begin{bmatrix} c\Omega c\omega - s\Omega s\omega ci & -c\Omega s\omega - s\Omega c\omega ci & s\Omega si \\ s\Omega c\omega + c\Omega s\omega ci & s\Omega s\omega + c\Omega c\omega ci & -c\Omega si \\ s\omega si & c\omega si & ci \end{bmatrix} \tag{5.7}$$

with c and s representing sin and cosine of the appropriate angles. The transpose of above is used to convert from ECI to perifocal. Transforming the formation reference frame to perifocal is done by

$$\left[\frac{PQW}{RSW}\right] = \begin{bmatrix} \cos\nu & -\sin\nu & 0 \\ \sin\nu & \cos\nu & 0 \\ 0 & 0 & 1 \end{bmatrix} \tag{5.8}$$

with the transpose used for moving in the other direction.

The algorithm used to calculate J_2 from the relative positions of the swarm satellites begins with converting relative positions into inertial positions.

$$\mathbf{R}^N = \left[\frac{PQW}{IJK}\right]\mathbf{R}_{ref} + \left[\frac{PQW}{IJK}\right]\left[\frac{RSW}{PQW}\right]\mathbf{r} \tag{5.9}$$

The next step is to calculate the accelerations in the inertial frame according to equations (5.3) through (5.5). These inertial accelerations can now be transformed, using equation (4.15) into the relative accelerations. Of note is the use of a static reference orbit. That is, the reference orbit is assumed to be unperturbed.

3. Comparison Between Sets of Equations.

Initial results from a comparison between the linear equations and the non-linear equations were encouraging. The comparison was done for a circular formation, with $e = 0$ at three different inclinations: 28.5º, 45º, and 63.4º. Figure V-1 to Figure V-3 show the perturbation accelerations due to J_2 effects for all three inclinations, normalized by the

scaling scheme detailed in section II.B.2. Figure V-4 to Figure V-6 show the difference between equation (5.1) and equations (5.3) through (5.5) for each inclination. Note that the differences are not random, but seem to follow some pattern. This is the effect of the higher order terms not present in the linear equations.

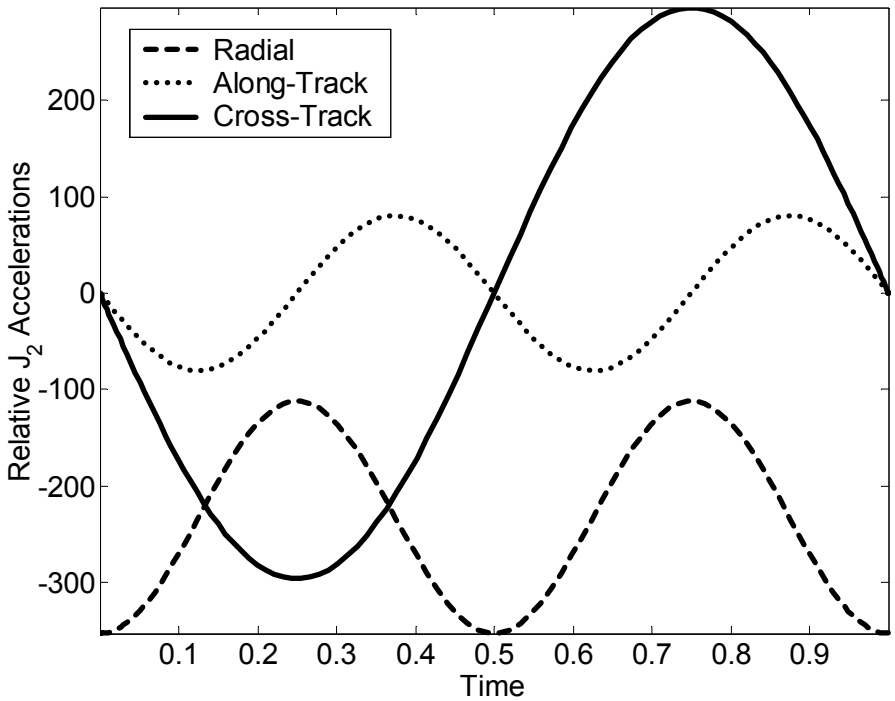

Figure V-1 Relative Accelerations Due to J2 at 28.5º Inclination

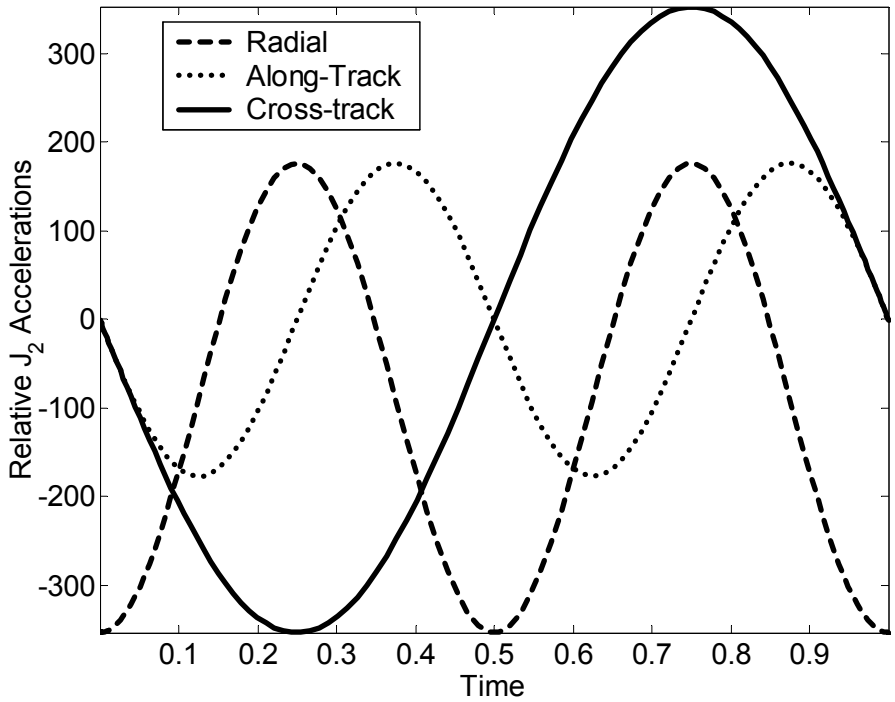

Figure V-2 Relative Accelerations Due to J2 at 45º Inclination

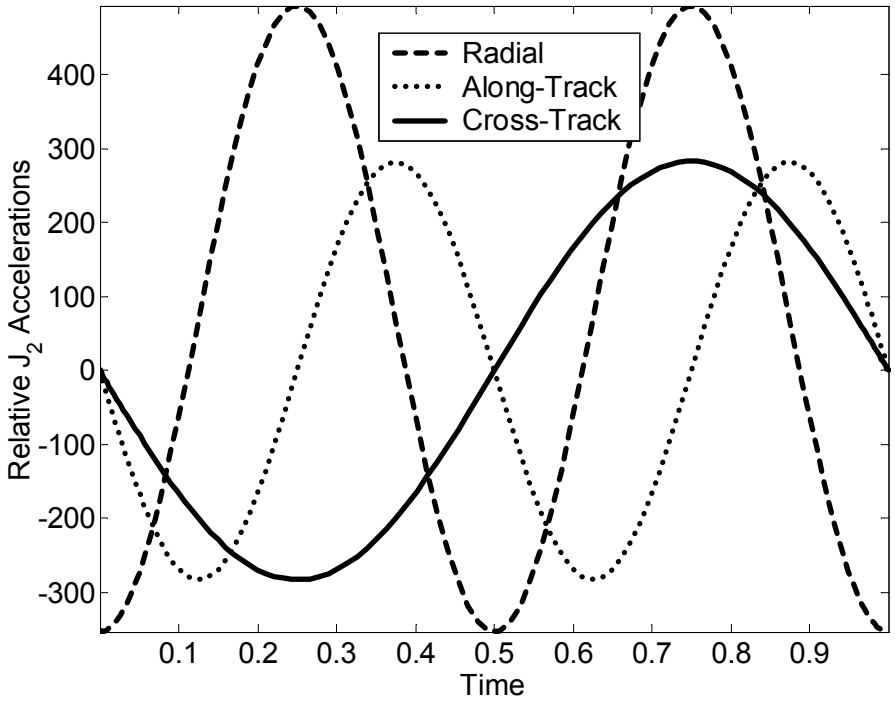

Figure V-3 Relative Accelerations Due to J2 at 63.4º Inclination

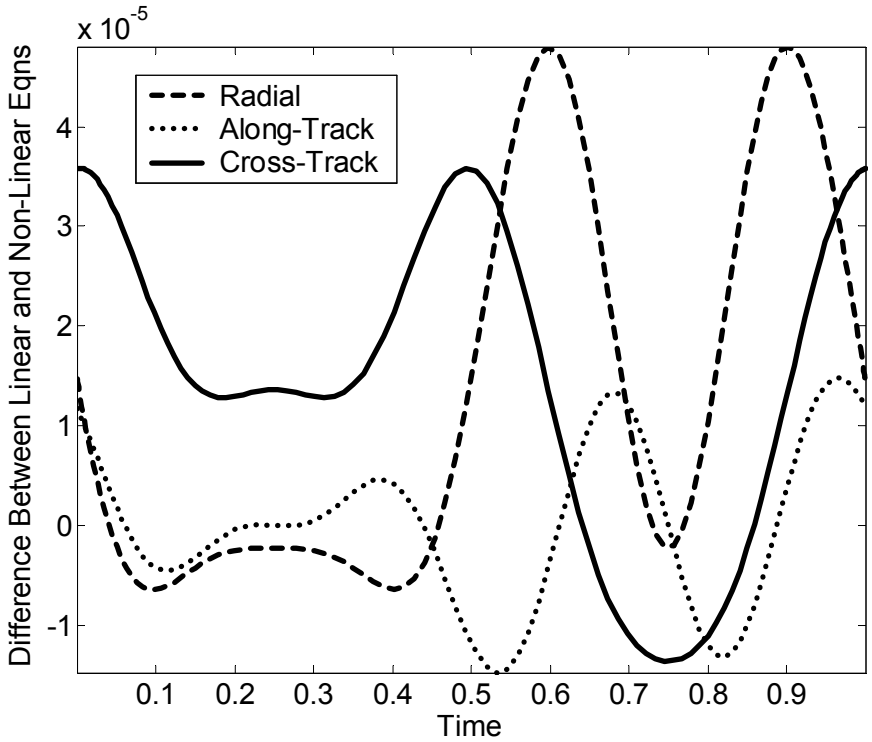

Figure V-4 Error in Linear Equations at 28.5º Inclination

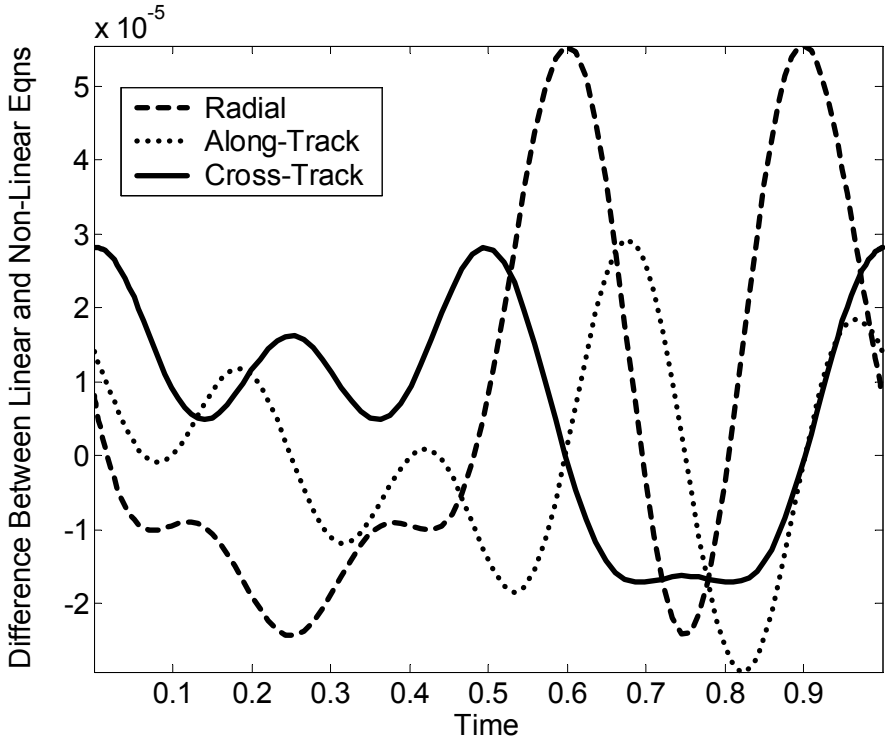

Figure V-5 Error in Linear Equations at 45º Inclination

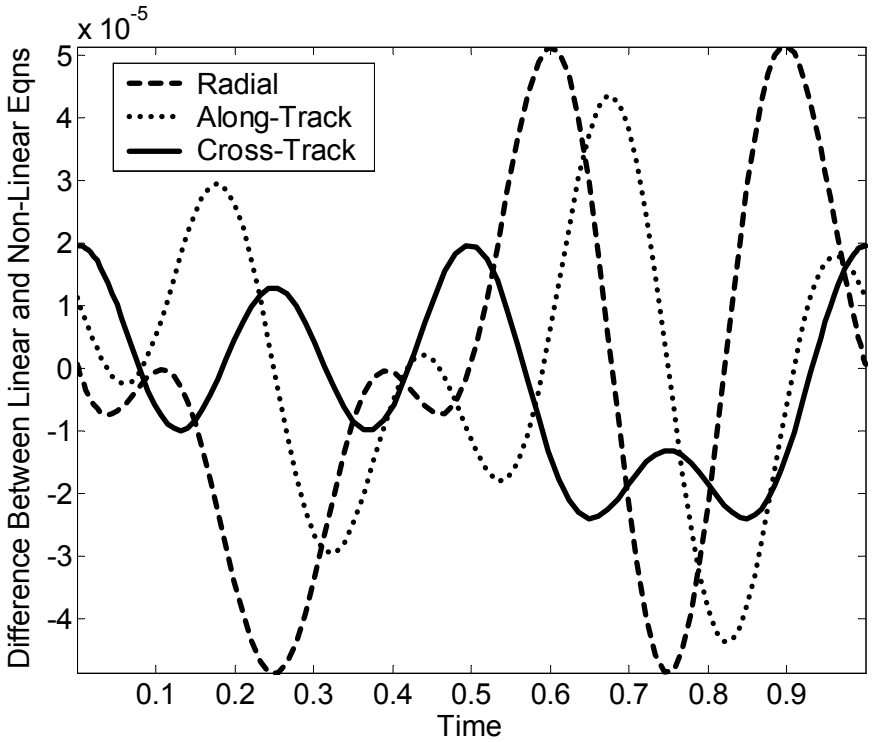

Figure V-6 Error in Linear Equations at 63.4º Inclination

VI. CONCLUSIONS AND FUTURE WORK

A. CONCLUSIONS

This work for this thesis started as a question: Can optimal periodic control (OPC) theory be applied to satellite formation design and control? Using the fundamentals of optimal control theory, a framework was developed that captures the essence of designing and controlling spacecraft formations. This framework is used to articulate a variety of formations including the notion of an aperiodic formation. Based on a deliberate formulation, including mass as a state variable, it was shown that the numerical approach can easily handle nonlinearities. Additionally, formations were presented that require active control along with their corresponding thrust profile.

This thesis lends credence to the notion of numerically searching for minimum-fuel formation configurations for spacecraft swarm subject to *arbitrary* nonlinear dynamics. Thus, practical formations may be designed and controlled using this method. The foundation for applying OPC to satellite formations has been completed. Future work can build on this foundation in increasing the complexity of the models. A substantial amount of work needs to be done in developing a more complete model of satellite motion and perturbations. The framework developed here can be readily used with more robust dynamical models and should produce very interesting results.

B. OPPORTUNITIES FOR FUTURE WORK

In addition to the topics identified in the previous chapters, opportunities for future work are available in the following areas.

In the course of implementation for Chapter IV, an additional "state" was added to simplify the equations. This state variable was ν with its corresponding derivative, $\dot{\nu}$. This required adding dynamical constraints for this state. One opportunity for future work would be to include ν in the path constraints and rewrite the dynamical equations to remove explicit dependence on ν. This may possibly increase numerical accuracy when implementing the model in DIDO.

Another possibility for follow on research is an examination of the ${}^{N}\dot{\omega}^{B}$ term . It may be possible to continue working in the formation reference frame, while adding the J2 effects to this term by including $\frac{d\Omega}{dt}$, $\frac{di}{dt}$, and $\frac{d\omega}{dt}$.

A departure from the relative reference frame would be an area for future work. The creation of a model in an inertial frame and the use of the full non-linear equations will create a high fidelity model, and will allow the addition of J2 effects and any other Earth-centered effects to be included more readily. Translating the formation constraints from the relative frame, where they are intuitive, to the inertial frame should be straightforward but tedious. If the model is defined in inertial space, the deployment and reconfiguration problems becomes a simple change from one orbit to another orbit. The difficulty lies in specifying the constraints, if any, on the reconfiguration relative motion and visualization.

Another consideration, offered by Dr. Terry Alfriend, is to write the path constraint as follows, and minimize total thrust.

$$\left(\frac{r_x}{\left|R_{ref}\right|}\right)^2 + \left(\frac{r_y}{\left|R_{ref}\right|}\right)^2 + \left(\frac{r_z}{\left|R_{ref}\right|}\right)^2 = constant \tag{6.1}$$

If the reference orbit is circular, then R_{ref} is constant and becomes a simple scaling factor, which was completed previously. The above constraint was not addressed for an elliptical reference orbit, where R_{ref} is no longer a constant.

Other unexplored areas include the possibility of near-circular relative formations. If a small deviation is allowed in the path, it may lower the cost of the formation. In addition, specific missions require specific configuration constraints. One very interesting area of research would be to identify and catalog various configuration constraints according to mission.

LIST OF REFERENCES

1. DeCou, A. B., "Orbital Station-Keeping for Multiple Spacecraft Interferometry," *Journal of Astronautical Sciences*, Vol. 39, July-Sept, 1991, pp. 283-297.

2. Leitner, J., (GSFC DSS Lead), Distribuited Spacecraft Systems, Technology Development Program, Goddard Space Flight Center, April, 2001.

3. Lau, K., et al, "The New Millennium Formation Flying Optical Interferometer," *AIAA Guidance, Navigation and Control Conference*, August 1997. Paper No. AIAA 97-3820.

4. Panetta, R. V., et al, "NASA-GSFC Nano-Satellite Technology Development," *AIAA/USU Small Satellite Conference*, August, 1998, Paper No. SSC98-VI-5.

5. Weidow, D. Bristow, J., "NASA/DoD University Nano-Satellites for Distributed Spacecraft Control," *AIAA/USU Small Satellite Conference*, August, 1999, Paper No. SSC99-V-5.

6. Vincent, M. A. and Bender, P. L., "The Orbital Mechanics of a Space-Borne Gravitational Wave Experiment," *Advances in the Astronautical Sciences, Astrodynamics*, 1987, Vol. 65, Part II, Pg. 1346. Edited by Soldner, J.K. et al. Paper AAS 87-523. Full paper in AAS Microfiche Series, Vol.55.

7. Bender, P. L. et al, "LISA: Laser Interferometer Space Antenna, Pre-Phase A Report," Second Edition, Jet Propulsion Laboratory, Report MPQ 233, Pasadena, CA, July 1998.

8. Schaub, H. and Alfriend, K. T., "J2 Invariant Reference Orbits for Spacecraft Formations," *1999 Flight Mechanics Symposium*, GSFC, May 18-20 1999.

9. Alfriend, K. T., Schaub, H. and Gim, D.-W., "Gravitational Perturbations, Nonlinearity and Circular Orbit Assumption Effects on Formation Flying Control Strategies," *23rd Annual AAS Guidance and Control Conference*, Breckenridge, CO, Feb.2-6 2000. Paper No. AAS 00-012.

10. McCall, G. H. (Study Director), New World Vistas, Summary Volume, USAF Scientific Advisory Board, December 1995.

11. Ross, I. M., Yan, H. and Fahroo, F., "A Curiously Outlandish Problem in Orbital Mechanics," *AAS/AIAA Astrodynamics Specialist Conference*, Quebec City, Canada, July 2001.

12. Strizzi, J., Ross, I. M. and Fahroo, F., "Towards Real-Time Computation of Optimal Controls for Nonlinear Systems," *AIAA Guidance, Navigation and Control Conference*, Monterey, CA 2002. Paper No. AIAA 2002-4945.

13. Ross, I. M. and Fahroo, F., "A Pseudospectral Transformation of the Covectors of Optimal Control Systems," *Proceedings of the First IFAC Symposium on System Structure and Control*, Prague, The Czech Republic, August 2001.

14. Ross, I. M. and Fahroo, F., "User's Manual for DIDO 2001: A MATLAB Application Package for Dynamic Optimization," *NPS Technical Report AA-01-003*, Department of Aeronautics and Astronautics, Naval Postgraduate School, Monterey, CA, December 2001.

15. Clohessy, W.H. and Wiltshire, R. S., "Terminal Guidance System for Satellite Rendezvous," *Journal of the Aerospace Sciences*, Vol.27, No. 9, Sept. 1960, pp. 653-658.

16. Carter, T. E., "New Form for the Optimal Rendezvous Equations near a Keplerian Orbit," *Journal of Guidance, Control, and Dynamics,* Vol. 13, No. 1, 1990, pp. 183-186.

17. Inhalan, G., Tillerson, M., and How, J. P., "Relative Dynamics and Control of Spacecraft Formations in Eccentric Orbits," *Journal of Guidance, Control, and Dynamics,* Vol. 25, No. 1, 2002, pp. 48-59.

18. Melton, R., "Time-Explicit Representation of Relative Motion Between Elliptical Orbits.," *Journal of Guidance, Control, and Dynamics,* Vol. 23, No. 4, 2000, pp. 604-610.

19. Ross, I. M., King, J. T. and Fahroo, F., "Designing Optimal Spacecraft Formations," *AIAA Guidance, Navigation and Control Conference*, Monterey, CA 2002. Paper No. AIAA 2002-4635.

20. Vallado, D. A., *Fundamentals of Astrodynamics and Applications*, Second Edition, Space Technology Library, Microcosm Press, El Segundo, CA, 2001.

21. Vinter, R. B., *Optimal Control*, Birkhauser, Boston, MA, 2000.

22. Betts, J. T., *Practical Methods for Optimal Control Using Nonlinear Programming*, SIAM: Advances in Control and Design Series, Philadelphia, PA, 2001.

23. Bryson, A.E., and Ho, Y.C., *Applied Optimal Control*, Hemisphere, New York, 1975.

24. McLaughlin, C. A, Sabol, C., Swank, A., Burns, R. D., Luu, K. K., "Modeling Relative Position, Relative Velocity, and Range Rate for Formation Flying," *Advances in the Astronautical Sciences, Astrodynamics*, 2001, Vol. 109, Part III, AAS 01-456.

25. Pollard, J. E., Chao, C. C., and Janson, S.W., "Populating and Maintaining Cluster Constellations in Low-Earth Orbit." *AIAA/ASME/SAE/ASEE Joint Propulsion Conference*, Los Angeles, CA 1999. Paper No. AIAA-99-2871.

26. Chichka, D. F., "Satellite Clusters with Constant Apparent Distribution," *Journal of Guidance, Control, and Dynamics*, Vol. 24, No. 1, 2001, pp. 117-122

27. Yamanaka, K., and Ankersen, F., "New State Transition Matrix for Relative Motion on an Arbitrary Elliptical Orbit," *Journal of Guidance, Control, and Dynamics*, Vol. 25, No. 1, 2002, pp. 60-66.

28. Kane, T. R., Likins, P. W., and Levinson, D. A., *Spacecraft Dynamics*, McGraw-Hill Book Co., New York, 1983, pg. 213.

29. Bate, R. R., Mueller, D. D., White, J. E., *Fundamentals of Astrodynamics*, Dover Publications, Inc., New York, 1971, pp. 399

30. Ross, I. M., "Linearized Dynamical Equations for Spacecraft Subject to J_2 Perturbations," to appear in *Journal of Guidance, Control, and Dynamics.*

THIS PAGE INTENTIONALLY LEFT BLANK

INITIAL DISTRIBUTION LIST

1. Defense Technical Information Center
   Ft. Belvoir, Virginia

2. Dudley Knox Library
   Naval Postgraduate School
   Monterey, California

3. Professor I. Michael Ross
   Naval Postgraduate School
   Monterey, California

4. Professor Fariba Fahroo
   Naval Postgraduate School
   Monterey, California

5. Julian King
   Modesto, CA.

6. Jeffery T. King
   SPAWAR SFA
   Warrenton, VA.